Front. Energy 2021, 15(3): 600–620
https://doi.org/10.1007/s11708-021-0737-0

REVIEW ARTICLE

Bing LUO, Yuxin ZHAO, Dengwei JING

State-of-the-art progress in overall water splitting of carbon nitride based photocatalysts

Abstract Converting solar energy into hydrogen (H_2) by photocatalytic water splitting is a promising approach to simultaneously address the increasing energy demand and environmental issues. Half decade has passed since the discovery of photo-induced water splitting phenomenon on TiO_2 photoanode, while the solar to H_2 efficiency is still around 1%, far below the least industrial requirement. Therefore, developing efficient photocatalyst with a high energy conversion efficiency is still one of the main tasks to be overcome. Graphitic carbon nitride (g-C_3N_4) is just such an emerging and potential semiconductor. Therefore, in this review, the state-of-the-art advances in g-C_3N_4 based photocatalysts for overall water splitting were summarized in three sections according to the strategies used, and future challenges and new directions were discussed.

Keywords photocatalysis, overall water splitting, carbon nitride, hydrogen

1 Introduction

Efficient utilization of solar energy has been widely regarded as a promising way to solve the increasing energy demand and environmental concerns caused by the burning of fossil fuels. Because the solar energy striking on the earth surface is about 1.3×10^5 TW/a, and far exceeds the global human energy consumption of 2013 (approximately 17 TW), which is predicted to at least double by 2050, by roughly four orders of magnitude [1,2]. In 1972, Fujishima and Honda discovered the water splitting phenomenon on an ultraviolet (UV) light irradiated TiO_2 electrode [3], henceforth, using solar light driven water splitting to convert and store solar energy in chemical fuel (H_2) has attracted worldwide attention.

Photovoltaic-electrolysis (PVE) [4,5], photoelectrochemical (PEC) catalysis [1,6], and photocatalysis (PC) [1,7] are the three main sunlight driven approaches to produce H_2 from water. Therein to, PVE has the highest solar-to-hydrogen (STH) efficiency while it suffers from the high cost competitive to nowadays industrial methane steam reforming process. Techno-economical analyses of the PEC and the PC system predict that H_2 production cost would approximate 4.10–10.40 $/kg and 1.60–3.20 $/kg, respectively, if a similar STH is achieved. Obviously, PC has the lowest cost which also meets the requirement of DOE predicted target H_2 price (2.00–4.00 $/kg) [8]. Moreover, the particulate PC system is a more low-cost technology with the potential to enable large-scale application, because of the ready synthesis of the associated photocatalysts as well as the simple reactor and facility designs [9]. However, the low STH efficiency of the PC system is the main factor restricting industrial application. According to the prediction by the US Department of Energy (DOE), STH should at least reach around 10% to meet the basic requirement for large-scale utilization in an acceptable cost [7,8]. Up to now, the highest STH achieved is around 1%, which is far below the lowest requirement [8,10]. Rationally designing and developing more efficient photocatalysts to promote STH efficiency is still the primary demand of a photocatalytic H_2 production based PC system.

Adding sacrificial reagents into the PC system to immediately consume photo-induced holes (electrons) is effective to prolong charge carrier lifetime, thus, providing enough time for charge carrier to participate in water

Received Nov. 16, 2020; accepted Dec. 10, 2020; online Apr. 25, 2021

Bing LUO, Yuxin ZHAO (✉)
School of Chemical Engineering and Technology, Xi'an Jiaotong University, Xi'an 710049, China
E-mail: yuxinzhao@mail.xjtu.edu.cn

Dengwei JING (✉)
International Research Center for Renewable Energy and State Key Laboratory of Multiphase Flow in Power Engineering, Xi'an Jiaotong University, Xi'an 710049, China
E-mail: dwjing@mail.xjtu.edu.cn

Special Issue—Photocatalysis: From Solar Light to Hydrogen Energy (Guest Editors: Wenfeng SHANGGUAN, Akihiko KUDO, Zhi JIANG, Yuichi YAMAGUCHI)

reduction (oxidation) reaction to generate H_2 (O_2). Photocatalytic H_2 (O_2) production in the presence of sacrificial regents is also called sacrificial half-reaction. However, photocatalytic half-reaction might be a downhill process due to the consumption of sacrificial reagent, namely, the solar energy may be not stored in the H_2 produced [8]. Meanwhile, using sacrificial reagents to trap photo-induced charge may increase the cost of the H_2 produced. Hence, it is necessary to photocatalyze water splitting at a high STH efficiency without bringing in any sacrificial reagents.

2 Basis of photocatalytic overall water splitting

Photocatalytic overall water splitting is an uphill reaction ($H_2O = H_2 + 1/2O_2$, $\Delta G° = 237$ kJ/mol) with increased Gibbs free energy. Generally, the process from input solar energy to the final output H_2 energy can be divided into three primary processes as shown in Fig. 1. Step 1, semiconductor photocatalyst absorbs incident photons with a higher energy than the band gap and generates charge carriers (electron-hole pairs). Step 2, electron-hole pairs separate and transfer to the catalyst surface, and ready to react with adsorbed reactant molecules. Step 3, electrons and holes participate in H_2 evolution reaction (HER) and O_2 evolution reaction (OER), respectively. In Step 1, the conduction band (CB) minimum and valence band (VB) maximum of a photocatalyst should straddle the potential of H^+/H_2 (0 V versus NHE) and O_2/H_2O (1.23 V versus NHE). From the thermodynamic viewpoint, the smallest band gap of a photocatalyst for the one-step overall water splitting should be 1.23 eV. However, in practice, due to the existence of over-potential both in reduction and oxidation half reaction, the semiconductor band gap should be larger than approximaely 1.6 eV that can drive the one-step overall water splitting. Moreover, it is worth noting that if the band gap is larger than 3.2 eV, only UV light can be absorbed to drive water splitting reaction. However, the energy of UV light only occupies approximaely 5% of the total energy of solar spectrum. Consequently, in terms of absorbing and using solar energy as more as possible to fulfill industrial STH efficiency, developing highly efficient visible light responsive photocatalysts is the primary strategy to reach this goal. To this end, GaN:ZnO [11,12], $SrTiO_3$:Rh/$BiVO_4$ [10,13], (oxy)sulfide [14], g-C_3N_4 [15,16], etc. have been developed, all of which exhibit great potential for overall water splitting. Here, this review just focuses on recent progresses in g-C_3N_4 based photocatalysts in this field.

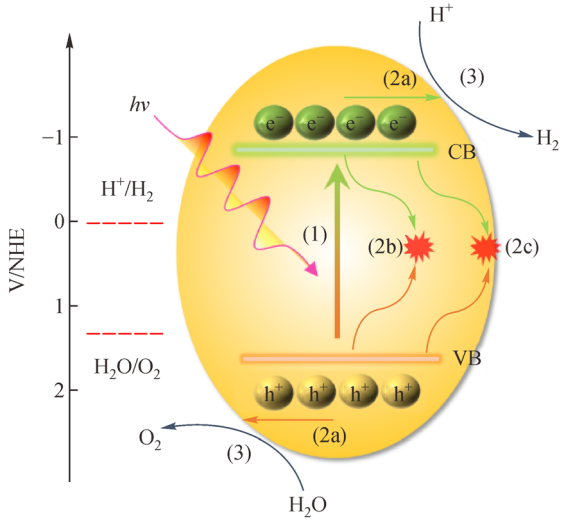

Fig. 1 Overall water splitting reaction on a photocatalyst. (1): Formation of photo-induced electron-hole pairs under light irradiation with photo-energy higher than the semiconductor band gap; (2): The charge separation/transfer/recombination: (2a)—electrone/holes moving to catalyst surface and ready to react with reactants; electrons and holes recombining with each other; (2b)—in the bulk; (2c)—at the surface; (3): Electrons and holes participating in water redox reaction to evolve H_2 and O_2, where cocatalysts being always loaded to facilitate the overall reaction.

3 Brief introduction to g-C_3N_4

3.1 g-C_3N_4

An ideal C_3N_4 nanosheet consists of C and N atoms that form the tri-s-triazine (heptazine) or triazine periodic units by sharing N atoms (Fig. 2(a)). The C_3N_4 nanosheet further bounds with adjacent layers by Van der Waals interaction to form a graphite-like layered structure [17–19], also known as graphitic carbon nitride (g-C_3N_4, hereinafter labeled as CN). Although triazine based CNs have also been reported for photocatalysis, yet, tri-s-triazine based CN is energetically favored and more stable [20]. CN can be facilely synthesized through a thermal polymerization process of N-rich molecule monomers, such as urea, melamine, cyanamide, and dicyanamide, etc [16,21–23]. Ong et al. summarized the detailed discovery and development of CN based on a series of pioneering work [16]. In the present paper, in particular, cyanamide is taken out as the typical precursor to elucidate the intermediates evolution from initial precursor to final product during the thermal polymerization process. Wang et al. combined thermogravimetric analysis (TGA) with X-ray diffraction (XRD) to monitor the decomposition and formation of intermediates related to reaction temperature [24], according to which, in the temperature range from 203°C to 335°C, cyanamide started to condense to form dicyandiamide and further form melamine accompanied with the releasement of NH_3. Subsequently, melamine molecules rearranged and constructed the tri-s-triazine unit at 390°C. The polymerization of tri-s-triazine commenced around 520°C and produces the polymeric CN. The polymeric

product became unstable above 600°C, and completely decomposed beyond 700°C.

3.2 Basic physical and chemical properties

The band gap of bulk CN is experimentally determined as approximately 2.7 eV, enabling visible light absorption up to approximately 460 nm. Density functional theory (DFT) calculations and experimental investigations reveal that the lowest unoccupied molecular orbital (LUMO) and the highest occupied molecular orbital (HOMO) are mainly composed of N p_Z orbitals and C p_Z orbitals, respectively, and straddle the H^+/H_2 and O_2/H_2O potentials. Therefore, on the one hand, the energy band structure is proper for overall water splitting (Figs. 2(b) and 2(c)) [25]. On the other hand, the light-trigged electrons and holes are mainly distributed around N and C atoms, respectively, indicating that the reduction and oxidation process for splitting water occur spatial independently [26]. In addition to suitable energy band structure, low cost, environmental tolerance, and facile synthesis methodology, the graphite-like layered structure and weak Van der Waals interaction between adjacent layers make CN aggregates to be easily exfoliated into single or few layered nanosheets. The CN nanosheets with a thinner lateral thickness render the photo-induced charge carriers sustaining short migration distance, representing a higher separation and transfer efficiency from the formation sites to the reaction sites. Moreover, nanosheets can provide more reaction sites and have the potential to construct functional nanohybrids with other components [27]. In view of the above discussion, CN nanosheets preparation and subsequent usage in catalytic applications have drawn numerous interest due to the unique merits of two dimensional (2D) materials [28–31].

In spite of the tremendous fascinating advantages of CN in photocatalytic water splitting, several disadvantages seriously restrict the STH efficiency improvement. In particular, the incomplete polymerization of amino groups leads to a high bulk defect density that indicates more electron-hole recombination centers. In addition, the charge transfer between two layers, bounded by the weak Van der Waals force, needs to overcome a large potential barrier [19]. Both of the above two factors heavily decrease the possibility of photo-induced charge carriers moving from the forming sites to the surface reaction sites. Therefore, researchers have made numerous efforts to address these issues for improving the catalytic performance, and the solar-driven overall water splitting is no exception. To the best of the authors' knowledge, the review of the advancements of CN based photocatalysts for photocatalytic overall water splitting has not yet been reported. Therefore, it is of great significance to summarize the advances, which can, in turn, contribute to the development in this field. Additionally, it is also necessary to discuss future prospects and challenges of CN based catalysts for photocatalytic overall water splitting.

4 Recent progress on overall water splitting of CN based photocatalysts

The photocatalytic overall water splitting activity of pristine CN is poor due to the lack of redox reaction sites and serious charge carrier recombination caused by the packed layers and incomplete thermal polymerization of amino groups. To overcome this problem, numerous strategies have been proposed to acquire a better performance. State-of-the-art advances are reviewed and discussed in three subsections, including loading cocatalysts, microstructure regulation and modification, and constructing nanocomposites.

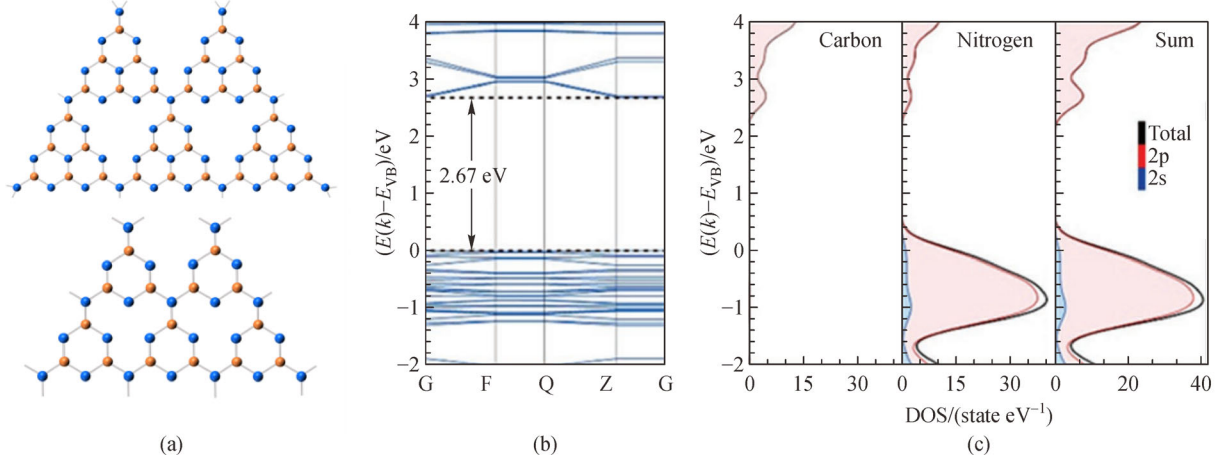

Fig. 2 Crystal and electronic structure of ideal C_3N_4 nanosheet.
(a) Illustration of CN layer formed by periodic units of tri-s-triazine (upper) or triazine (lower); (b) band structure; (c) partial density of states (PDOS) of CN (reproduced with permission from Ref. [25]).

4.1 Loading cocatalysts

Generally, loading cocatalyst on the surface of photocatalyst is beneficial for accelerating photocatalytic water splitting due to the synergy function of improving charge separation efficiency and acting as redox reaction sites. For example, in the presence of HER cocatalyst like noble metal Pt, photo-induced electrons are extracted by Pt nanoparticles due to the larger work function compared to the semiconductor photocatalyst, while the photo-induced holes still remain on the photocatalyst. Thus, it efficiently improves the charge carrier separation efficiency. On the other hand, Pt is an excellent H_2 evolution cocatalyst. The trapped electrons by Pt particles would be ready to reduce water into H_2. Eventually, the introduction of cocatalysts enhances the photocatalytic water splitting performance. Regarding pristine CN, the lack of photo-redox reaction sites and serious photo-generated charge carrier recombination heavily limit its catalytic performance. Therefore, it has a poor H_2 production activity in the half reaction, and almost no activity for photocatalytic overall water splitting. Consequently, in order to acquire the pure water splitting ability under solar light irradiation, integrating cocatalyst with CN is always an inevitable and efficient strategy. Recent advancement of cocatalysts modified CN for photocatalytic overall water splitting has been tabulated in Table 1.

4.1.1 Noble metals

Noble metals, such as Pt, Au, Ir, etc. have large work functions and thus possess excellent charge carrier trapping capacities [32]. Therefore, noble metal based materials are the most widely used cocatalysts for pure water splitting. For instance, *in situ* formed (111) facets-oriented noble Au nanoparticles on CN nanosheets achieves overall water splitting under visible solar light ($\lambda > 420$ nm) [33]. Benefiting from the extended light absorption because of the surface plasmon resonance (SPR) of Au, the Schottky barrier depressed charge recombination, and the proper band level alignment, the highest H_2 evolution rate of up to 150.1 μmol/(h·g) is obtained. In another case, IrO_2 quantum dots (approximately 2 nm) are deposited on protonated CN by a facile solvothermal method and play the role of oxidation reaction promotor [34]. Although the mass of IrO_2 is about 0.6 wt% in the hybrid, it, with a quite small size, can be highly dispersed and form an intimate contact with CN,

Table 1 Cocatalysts for photocatalytic overall water splitting over CN based photocatalysts

Cocatalyst	Light source	Efficiency	HER/(μmol·h^{-1})	H_2/O_2	Mass/mg	Ref.
IrO_2	300 W Xe lamp, $\lambda > 400$ nm	AQY: 2.1% not mention the light wavelength	45	2.25	30	[34]
Pt, PtO_x, and CoO_x	300 W Xe lamp, $\lambda > 300$ nm	AQY: 0.3% at 405 nm	12.2	1.94	200	[35]
Pt and CoP	300 W Xe lamp, $\lambda > 420$ nm	NA	2.1	2.10	80	[36]
Pt and Co_3O_4	300 W Xe lamp, $\lambda > 300$ nm	NA	3.1	2.10	20	[15]
Rh-RhO_x	300 W Xe lamp, $\lambda > 400$ nm	AQY: 0.1% at 420 nm	1.4	2.30	50	[37]
$PtMO_x$ and Co_3O_4	300 W Xe lamp, $\lambda > 420$ nm	AQY: 4.9% at 420 nm	2.38	1.99	50	[38]
Pt/$Ni(OH)_2$ and Pt	300 W Xe lamp	AQY: 4.2% at 420 nm	26.60	2.10	20	[39]
Pt and $Ni(OH)_2$	150 W Xe lamp, 200 nm $< \lambda <$ 2500 nm	AQY: 1.48% at 405 nm	15.5	1.99	200	[40]
Pt/$Ni(OH)_2$/CN	300 W Xe lamp	AQY: 1.8% at 420 nm	4.257	2.12	10	[41]
Pt-Au single-sites	300 W Xe lamp	AQY: 3% at 420 nm	8.55	2.00	30	[48]
Pt and Ru	Not mention, $\lambda > 350$ nm	NA	2.49	2.18	50	[49]
C dots	300 W Xe lamp, $\lambda > 420$ nm	AQY: 16% at 420 nm STH: 2%	~8.4	2.02	80	[50]
C dots	300 W Xe lamp, $\lambda > 420$ nm	NA	0.25	2.00	50	[51]
Amorphous NiO	300 W Xe lamp, 420 nm $< \lambda <$ 700 nm	NA	1.41	1.99	50	[52]
CoO	300 W Xe lamp, 420 nm $< \lambda <$ 700 nm	NA	0.46	2.19	80	[53]
MnO_2	300 W Xe lamp, $\lambda > 420$ nm	AQY: 3.82% at 420 nm	5.53	2.00	100	[54]
CNT and MnO_2	70 W metal halide lamp, 380 nm $< \lambda <$ 780 nm	NA	122	About 2.00	30	[55]
Mn_2Co_2C at C and MoOOH	300 W Xe lamp	AQY: 1.45% at 20 nm	8.876	2.05	150	[56]
Co_1-phosphide single sites	300 W Xe lamp, $\lambda > 300$ nm	AQY: 2.2% at 500 nm	8.206	2.00	20	[57]
WC_{1-x}	300 W Xe lamp, $\lambda > 420$ nm	AQY: 11.24% at 420 nm	3.364	2.02	40	[58]

thus significantly promoting the electron-hole separation efficiency and concurrently increasing the absorbance capacity of visible light. After IrO_2 modification, the H_2 and O_2 production rates can reach 45 μmol/h and 20 μmol/h under light with wavelength ($\lambda > 400$ nm), respectively.

In addition to Au and Ir based materials, cocatalysts containing Pt are the most widely used candidates in photocatalytic overall water splitting. However, in the sole presence of Pt, catalytic activity is obviously poorer than that in the multi-cocatalytic system, as multi-cocatalysts can facilitate H_2 and O_2 production separately due to the presence of respective components. Wang et al. have successfully decorated CN with Pt, PtO_x, and CoO_x as redox reaction sites via photo-deposition process [35]. Pt acts as HER cocatalyst, simultaneously, PtO_x and CoO_x facilitate O_2 evolution. At $\lambda > 300$ nm light illumination, 12.2 μmol/h and 6.3 μmol/h of H_2 and O_2 evolution rates are obtained without adding any sacrificial reagents (apparent quantum yield (AQY): 0.3% at 405 nm). Further, they constructed another multi-cocatalytic system by CoP and Pt [36]. Dual cocatalysts forming heterojunctions with CN display a two times catalytic performance improvement compared to Pt/CN. After introducing CoP, the water oxidation process is evidently accelerated by promoting the charge carrier separation efficiency. Moreover, Co_3O_4 and Pt nanoparticles are separately deposited on the outer and inner surface of hollow CN spheres by using mesoporous-SiO_2 as hard template (Figs. 3(a) and 3(b)) [15]. The spatially separated HER and OER reactive sites accept the unidirectional migration of electrons and holes on the Janus surface, thereby decreasing charge recombination and preventing the unwanted reverse reaction of water splitting. The delicately designed Co_3O_4/HCNS/Pt photocatalyst has a 3.1 μmol/h H_2 evolution rate and a 1.5 μmol/h O_2 evolution rate. The gas evolution rate is about 10 times faster than that of pure HCNS, and it is also much better than Co_3O_4 and Pt co-modified HCNS without spatial separation (Figs. 3(c) and 3(d)). The selective deposition of HER and OER cocatalysts for promoting overall water splitting performance is further supported by

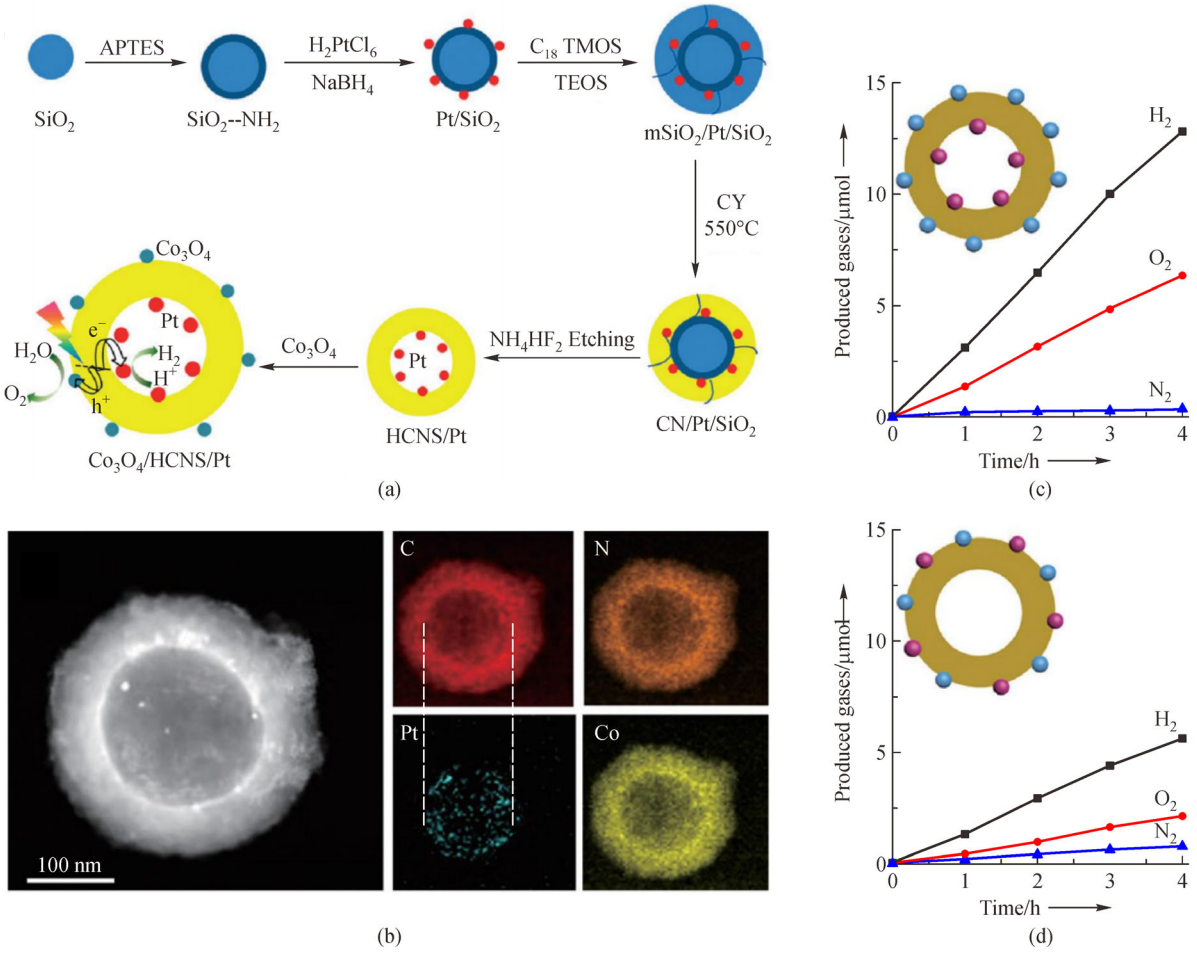

Fig. 3 Co_3O_4 and Pt coloaded hollow CN sphere for photocatalytic overall water splitting.
(a) Illustration of Co_3O_4/HCNS/Pt preparation process; (b) elemental mapping of Co_3O_4/HCNS/Pt; (c) time course of photocatalytic H_2 and O_2 evolution of Co_3O_4/HCNS/Pt under light irradiation ($\lambda > 300$ nm); (d) time course of photocatalytic H_2 and O_2 evolution of (Co_3O_4 + Pt)/HCNS (reproduced with permission from Ref. [15]).

the Rh and RhO_x spatially co-loaded CN [37]. Rh-RhO_x/PCN shows the accelerated reaction kinetics and boosted photo-induced charge carrier separation, compared to that of Rh or RhO_x solely modified CN. Hence, it is reasonable to infer that depositing noble metal based cocatalysts or further combining them with other cocatalysts is an efficient strategy to convert solar energy into H_2 through water without adding sacrificial reagents.

Pt sub-nanoparticles which are deposited on alkali-metal-oxides that are intercalated in the CN layers, and Co_3O_4 particle co-deposition on CN can drive overall water splitting under visible light ($\lambda > 420$ nm) [38]. In the hybrid, the intercalated alkali-metal-atoms bridging two adjacent layers as charge conductor enable more efficient charge transportation and separation. In addition to accelerating H_2 production, Pt sub-nanoparticles also function as H_2 permeable membrane and prohibit the permeating of O_2, thus supressing their back reaction. With regard to the Co_3O_4 particles, they significantly facilitate the water oxidation process. In the Pt/$Ni(OH)_2$ nanowires and Pt nanoparticle co-modified system [39], abundant coordinatively unsaturated sites of Pt/$Ni(OH)_2$ effectively boost O_2 evolution, and Pt-O-Ni interactions retard O-O bond cleavage, thus inhibiting the backward H_2O regeneration. Furthermore, the Schottky junction formed by the isolated Pt with CN is beneficial for electron transfer and proton reduction. Ultimately, due to the improved charge separation, prohibited backward reaction, and tuned surface kinetics, stoichiometric H_2 and O_2 production rates of up to 26.60 and 12.64 μmol/h (AQY: 4.2% at 420 nm), are obtained respectively. Regarding another Pt decorated β-$Ni(OH)_2$/CN [40], β-$Ni(OH)_2$ nanolayers tune the water oxidation kinetics by decreasing OER overpotential and promoting the charge separation/transfer efficiency. Pt nanoparticles are *in situ* photo-deposited on CN surface, and significantly enhance H_2 evolution rate. Therefore, overall water splitting is achieved under solar light irradiation. Interestingly, the photo-induced Pt decorated $Ni(OH)_2$ can serve as a strong synergetic cocatalyst [41]. The intimate contact of nanosized Pt with $Ni(OH)_2$ brings up a strong $Pt^{\sigma+}$ -$O^{\sigma-}$ interaction, which enhances H_2O activation along with accelerated charge transfer/separation efficiency. This unique structure prefers to H_2O adsorption and further makes H-OH bonds more easily to be activated and cleaved. This work elucidates the importance of introducing H_2O activation component into the pure water splitting system.

Despite the excellent cocatalytic performance, however, the scarcity of noble metals on the earth leads to the high-cost in large-scale application. To keep the prominent cocatalytic ability and simultaneously reduce their cost, cutting large particles into smaller clusters and even isolated single atoms is an alternative and promising method. To this end, single noble metal atom modified photocatalysts have been developed and extensively investigated in overall water splitting, half reactions, and other fields [42–47]. In this paper, only the examples relating to overall water splitting over CN are summarized. Liu et al. have successfully modified CN by the atomically dispersed heterogeneous Pt_1N_x-Au_1N_x redox single sites. The formation of p-n coupled micro-domains as effective bifunctional electron-donor-acceptor centers evidently improves the electron-hole separation efficiency by 6–10 times relative to the individual Pt/CN and Au/CN [48]. Concurrently, a drastically reduced surface redox reaction barrier by approximately 300 mV of the bifunctional Pt-Au/CN single site photocatalyst is achieved. Under 300 W Xe-lamp irradiation, the introduction of Pt-Au single sites makes the hybrid successfully split pure water with 8.55 μmol/h of H_2 production rate (AQY: 3% at 420 nm) while it is of no activity for pristine CN.

Besides developing novel cocatalysts, addition of charge conductor (GO, carbon nanotubes, etc.) to connect photocatalyst and cocatalyst is proven to be effective for improving catalytic activity by tuning the charge transportation properties. One-dimensional carbon nanotube (1D CNT) modified 2D CN serves as a non-resonant plasmonic photocatalyst and produces H_2 and O_2 with the co-assistance of Pt and Ru [49]. The non-resonant plasmonic effect enhances the spectral response both in UV and visible light regions. Besides, the larger specific surface area, prolonged charge life time, and strong electronic coupling effect concurrently result in the considerable H_2 and O_2 production rate as 2.49 and 1.14 μmol/h, respectively.

4.1.2 Non-noble cocatalysts

Although noble metal single atoms or clusters has a prominent cocatalytic ability with significantly reduced cost, it is of more value to directly use earth-abundant elements to provide the same effect in good robustness. In the metal-free system, such as C dots embedded CN (Fig. 4(a)–4(f)), which is fabricated by heating the hybrids of ammonia treated C dots with urea [50], can stimulate photocatalytic overall water splitting through the stepwise two-electron/two-electron process: (i) $2H_2O \rightarrow H_2O_2 + H_2$, and (ii) $2H_2O_2 \rightarrow 2H_2O + O_2$. Therein to, CN is regarded to be responsible for the photocatalysis step (i) and C dots contribute to the second step (ii). Additionally, C dots are also beneficial for the light absorption. Eventually, C dots embedded CN displays a fantastic pure water splitting activity with approximately 8.4 μmol/h of H_2 production rate with H_2:O_2 as 2.02 (Fig. 4(g)). The AQY at 420 nm reaches 16% and STH is about 2% in the absence of any noble cocatalysts (Fig. 4(h)), representing that photocatalystic water splitting is rapidly proceeding toward industrial utilization [51]. In another case, to the same C dots/CN composite, it is synthesized by a thermal pyrolysis process, in which C dots are uniformly embedded into CN matrix and interacted by chemical bonding. The introduction of C dots effectively decreases

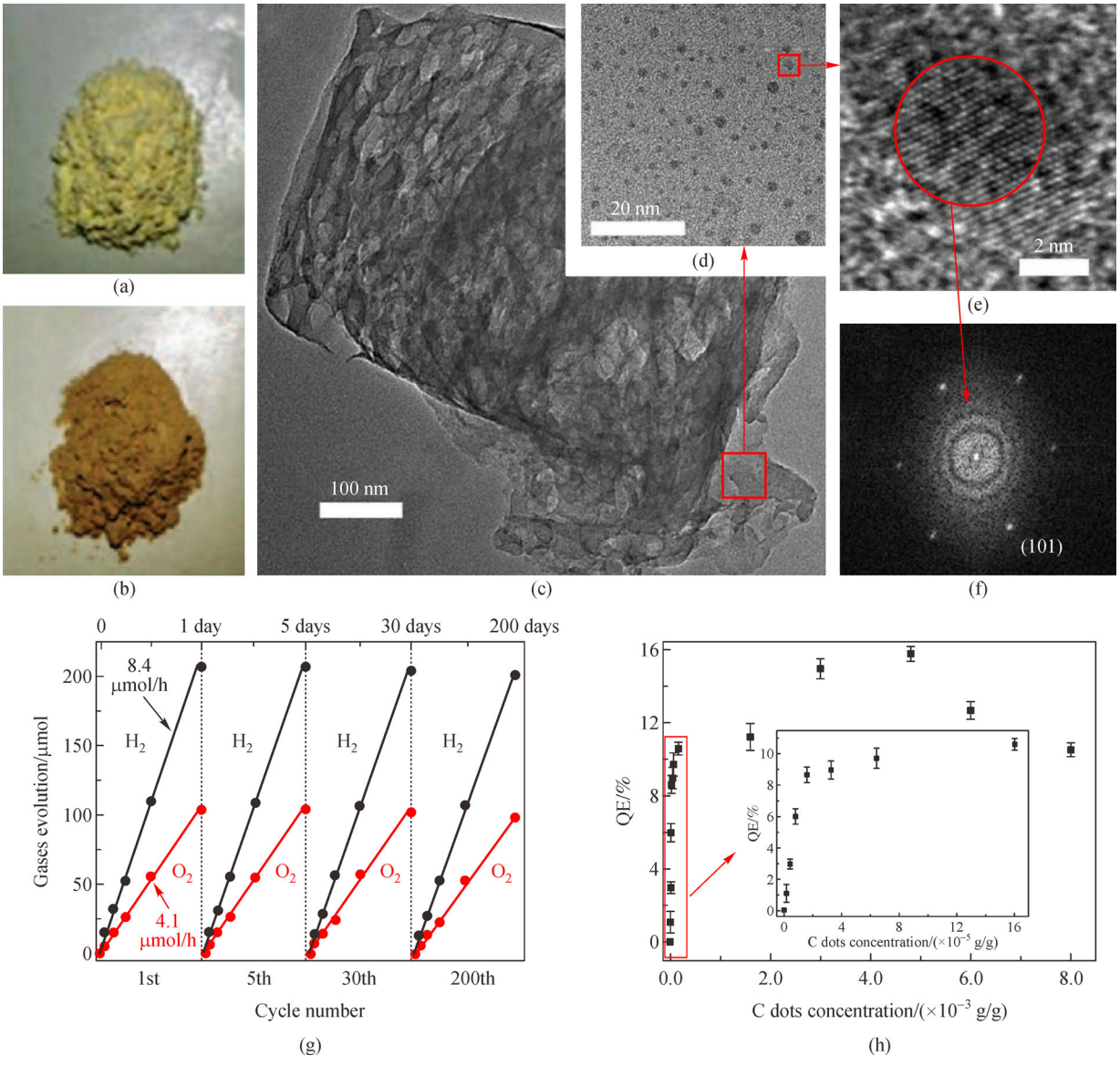

Fig. 4 C dots loaded CN composite for photocatalytic overall water splitting.
(a) CN; (b) C dots/CN; (c) TEM image of a grain of the C dots/CN composite; (d) magnified TEM image of C dots/CN, marked in red in (c); (e) high resolution transmission electron microscopy (HRTEM) image of a single C dot embedded in CN; (f) Fast Fourier Transform (FFT) pattern of the crystallite in (e), indicating hexagonal symmetry of C dot; (g) time course of H_2 and O_2 production from water under visible light irradiation ($\lambda > 420$ nm); (h) C dots concentration dependent quantum efficiency (QE) (red dots) of C dots/CN at 420 nm (reproduced with permission from Ref. [50]).

the band gap from 2.84 to 2.08 eV. Meanwhile, the photo-induced electrons are rapidly extracted by the C dots while the holes are still remained on CN, thus resulting in their improved separation efficiency and prolonged life time. Interestingly, it is found that one-third of C dots work as H_2O_2 decomposition catalyst and the others do as H_2 production cocatalyst.

Besides the metal-free cocatalysts, most reported coatalysts are synthesized based on transition metals. Among these, transition metal oxides are an important class of non-noble candidates. For instance, by optimising the amount of NiO and calcination temperature, amorphous NiO can efficiently accept photo-induced charge carriers from CN to improve the charge separation efficiency. Meanwhile, NiO provides more redox reaction sites and simultaneously contributes to H_2O_2 decomposition [52]. Therefore, under visible light ($420\ \text{nm} < \lambda < 700\ \text{nm}$), the H_2 and O_2 production rates of up to 1.41 and 0.71 μmol/h are achieved, respectively. Similar roles of CoO have also been reported [53]. MnO_2 can accelerate the OER process because of its good activity for H_2O_2 decomposition. Therefore, combining MnO_2 with CN can obtain overall water splitting [54]. Moreover, in the MnO_2 and CNT dual cocatalysts system [55], CNTs capture photo-induced electrons from CN and act as HER cocatalyst, and MnO_2 particles catalyze the decomposition of H_2O_2 to facilitate

O_2 evolution. The strengthened charge separation efficiency and bringing of cocatalytic effect concurrently trigger the overall water splitting reaction under light irradiation (380–780 nm). Dual non-noble metal cocatalyts, like MnOOH as HER cocatalyst and Mn_2Co_2C@C as OER cocatalyst, co-deposited CN also present a prominent photocatalytic overall water splitting activity [56]. Anchoring Mn_2Co_2C@C on CN can form Schottky junction to efficiently capture photo-induced electrons, thereby facilitating charge separation/migration. MnOOH is in favor of water adsorption and concurrently reduces the O_2 evolution overpotential. Therefore, a H_2 evolution rate of 8.876 μmol/h is achieved, which is higher than that of 1 wt% Pt loaded CN.

In a recently reported typical example, a single-site Co_1-phosphide configured CN is successfully prepared which exhibits the fantastic catalytic performance [57]. The P atoms partially substitute C atoms in triazine rings and contribute to the formation of Co_1-P_4 structure upon phosphidation (Fig. 5). The unique micro-structure effectively suppresses charge recombination and prolongs charge carrier lifetime by 20 times compared to pristine CN. Consequently, it shows a H_2 evolution rate of up to 8.206 μmol/h (AQY: 2.2% at 500 nm) with a stoichiometric O_2:H_2 ratio of 1:2 under simulated sunlight ($\lambda > 300$ nm). This work offers the guideline to design transition metal-based single-atom grafted overall water splitting photocatalysts. Furthermore, thermally polymerizing hexacarbonyl tungsten and melamine mixture can synthesize Pt-like WC_{1-x} modified 3D porous CN with ultrathin layers and nitrogen defects [58]. The specific surface area, light absorption, and charge carrier separation efficiency of the obtained product can be significantly improved. Density function theory (DFT) calculations reveal that the coexistence of WC_{1-x} and N defects makes electrons densely distributed around the Fermi level of CN, thus significantly accelerating the energy flowing from the light-induced excitons into H_2. Ultimately, the H_2 and O_2 production rates of the hybridized photocatalyst are respectively measured as 3.364 and 1.668 μmol/h under visible light ($\lambda > 420$ nm) in a stoichiometric ratio of 2:1.

In summary, depositing cocatalysts to enable CN to have a photocatalytic overall water splitting activity is always inevitable and effective, and of course has achieved great progress. However, the STH efficiency is still far below the industrial need. Therefore, developing more efficient, low cost, and stable cocatalyst is still the urgent task.

4.2 Microstructure regulation and modification

Regulating or modifying the microstructure of a photocatalyst is efficient to modulate the morphology and acquire desired optical and electronic properties, in particular, the flexible strucutre of CN makes the numerous investigation on microstructure modification possible. Generally, the regulation of intrinsic characteristics renders the improvement of photocatalytic performance by promoting charge carrier transfer properties. However, it is not an effective way to introduce redox reaction sites in the CN based system. In another word, despite the modification, it still has to load other cocatalysts to achieve overall water splitting for the most reported cases, except for a few instances as reviewed below. The reported cases that structure modulation enables CN to split pure water by photocatalysis have been summarized in Table 2.

4.2.1 Nanostructure modulation

Three dimensional (3D) porous CN nanosheets (3D CNNS) can be synthesized by a self-assembly of cyanuric acid with melamine, following the freeze drying and thermal polymerization processes [59]. The 3D CNNS has an interconnected open-framework assembled by highly crystalline ultrathin nanosheets, thus exhibiting a quite large specific surface area and providing a pathway for faster charge transport and separation. It achieves a H_2 and O_2 production of up to 5.07 and 2.455 μmol/h (AQY: 1.4% at 420 nm), respectively. Moreover, via successive sealed condensation and hydrothermal treatment, a 3D sea-urchin-like CN has been synthesized with numerous defects (C≡N), resulting in a narrowed band gap of approximately 2.0 eV [60]. The 3D sea-urchin-structure enlarges the specific surface area, provides more reaction sites, and enables more efficient photo-induced charge separation and migration. DFT calculation confirms that the existence of -OH, -C = O, and -C≡N tunes the d-band center of Pt atoms, which is beneficial for a better stabilization of adsorbates and a higher catalytic ability. After loading 3 wt% of Pt, H_2 and O_2 production rates respectively reach 1.04 and 0.51 μmol/h under visible light. The thermal treatment of alkali and CN mixture is effective in creating in-plane pores due to the alkali etching effect [61]. The alkali etched CN has a significant improvement over specific surface area and separation efficiency of photo-induced electron-hole pairs relative to the pristine CN. However, excessive alkali usage would, in turn, decrease visible light absorbance and further the photocatalytic activity. After loading Pt (2 wt%), the optimal sample splits pure water to generate reduction product H_2 and oxidation products O_2 and H_2O_2. Without loading OER cocatalytst (C dots), it prefers to produce H_2O_2 instead of O_2 because the two-electron process is much more thermodynamic preferable than that of four-electron process. With the co-assistance of C dots and Pt, visible light ($\lambda > 420$ nm) driven photocatalytic H_2 and O_2 production rates reach 9.34 and 4.68 μmol/h, respectively, which is about 24.6 times that of CN. Regarding 2D nanosheets, recently, femtosecond pulsed laser was successfully used to exfoliate graphitic CN [62]. During the preparation process, incident photons weak the Van der Waals interactions to achieve single or few layered nanosheets. Simultaneously, they break strong C-N

covalent bonds and cleave s-triazine units, thus introducing abundant -C≡N defects on the newly formed surface. Interestingly, -C≡N defects contribute to stabilizing Pt atoms, modulating the electronic properties, shifting down the band edge position. The highly dispersed Pt atoms provide more reaction sites and meanwhile supress the backward reaction of H_2 and O_2, whose production rates respectively reach 0.426 and 0.187 μmol/h in the presence of 1.4 wt% Pt. To the best of the authors' knowledge, 1 D and 0 D CN based catalysts have not yet been applied for photocatalytic overall water splitting.

Further proceeding the modification into the molecular level, heterostructural carbon rings (C_{ring}) have been successfully planted within CN layers (Fig. 6) [63]. The

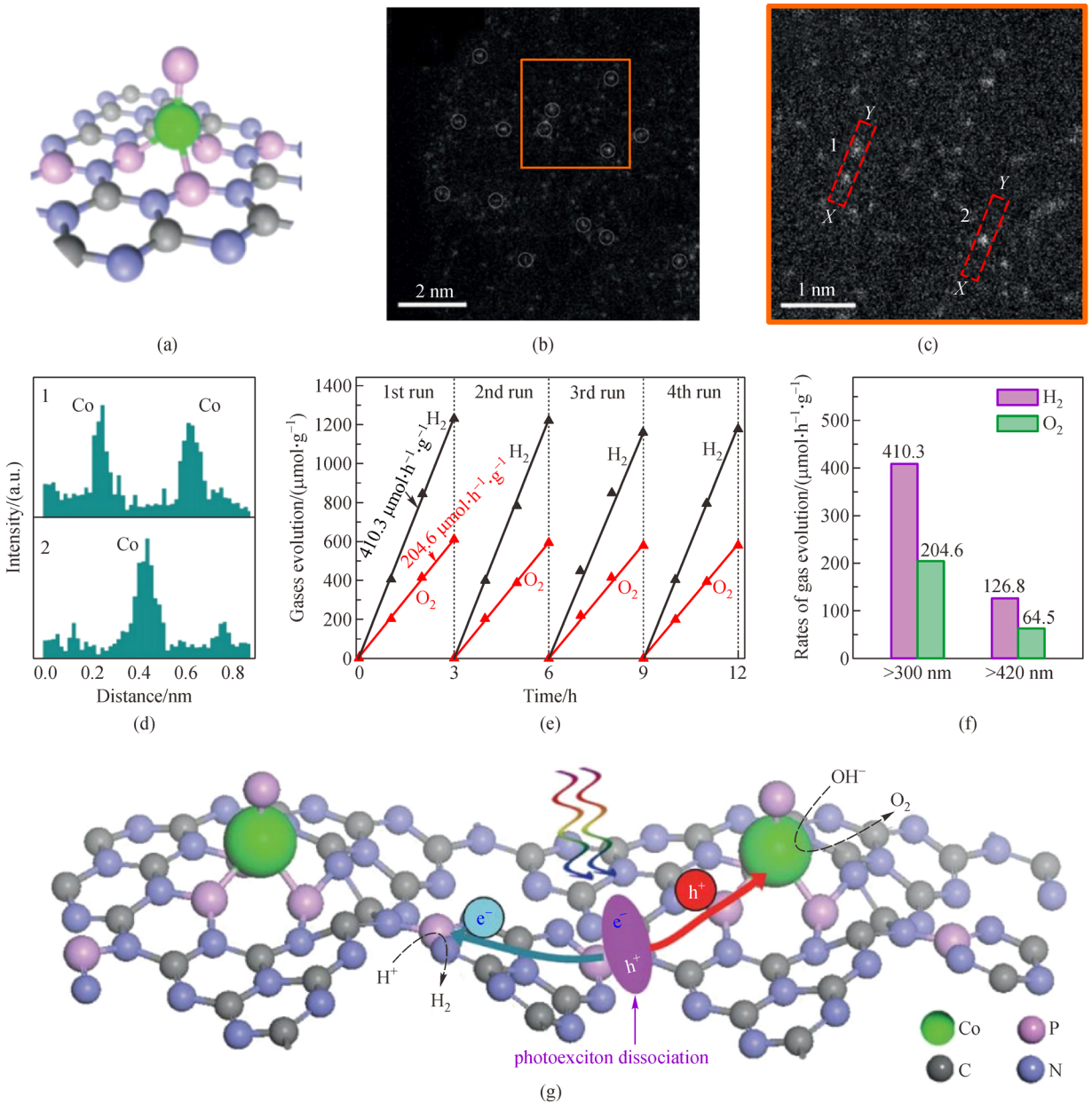

Fig. 5 Single site Co_1-phosphide modified PCN for photocatalytic overall water splitting.

(a) Schematic structural model for Co_1-phosphide/PCN; (b) High angle annular dark field-scanning transmission electron microscope (HAADF-STEM) image of Co_1-phosphide/PCN (isolated Co atoms are marked in white circles); (c) magnified HAADF-STEM image of the highlighted area in (b); (d) intensity profiles along lines *X*-*Y* at positions 1 and 2 in the HAADF-STEM image (c); (e) time course of H_2 and O_2 production from water splitting under light irradiation ($\lambda > 300$ nm) by Co_1-phosphide/PCN photocatalyst; (f) photocatalytic water-splitting activities under $\lambda > 300$ nm and $\lambda > 420$ nm light irradiation; (g) schematic illustration of solar-driven overall water splitting on Co_1-phosphide/PCN photocatalyst, where the photo-generated electrons and holes (h^+) are spatially separated, and transferred to active sites to drive HER and OER (Co green, P pink, N violet, C gray) (reproduced with permission from Ref. [57]).

Table 2 Nanosctructure modification of CN for photocatalytic overall water splitting

Sample	Light source	Efficiency	HER/(μmol·h^{-1})	H_2/O_2	Mass/mg	Other cocatalysts	Ref.
3D CNNS	300 W Xe lamp, $\lambda > 420$ nm	AQY: 1.4% at 420 nm	5.07	2.07	50	1 wt% Pt 3 wt% IrO_2	[59]
3D Sea-urchin-like CN	300 W Xe lamp, $\lambda > 420$ nm	AQY: 0.43% at 420 nm	1.04	2.04	25	3 wt% Pt	[60]
Alkali etched CN	300 W Xe lamp, $\lambda > 420$ nm	NA	9.34	2.03	10	2 wt% Pt CQDs	[61]
Laser exfoliated CN	300 W Xe lamp, $\lambda > 420$ nm	NA	0.426	2.28	10	1.4 wt% Pt	[62]
(C_{ring})-CN	300 W Xe lamp, $\lambda > 420$ nm	AQY: 5% at 420 nm	11.13	2.00	30	about 3 wt % Pt	[63]
C_{co}-CN	300 W Xe lamp	AQY: 5.28% at 400 nm	15.9	2.08	30	None	[64]
Benzene ring incorporated CN	300 W Xe lamp, $\lambda > 450$ nm	AQY: 2.1% at 450 nm	7	NA	5	1 wt% Pt	[65]
Na-CN	300 W Xe lamp, $\lambda > 420$ nm	AQY: 1.45% at 420 nm STH: 0.28%	31.5	2.07	100	1 wt% Pt	[66]
K/B co-doped CN	300 W Xe lamp, $\lambda > 400$ nm	NA	1.18	2.03	NA	None	[70]
PTI·HCl	300 W Xe lamp	AQY: 2.1% at 380 nm	about 65	about 2.00	100	1% Pt 9 wt% CoO_x	[75]
PTI-550	300 W Xe lamp	AQY: 8% at 365 nm	189	2.08	120	1wt% Pt 0.5 wt% Co	[76]

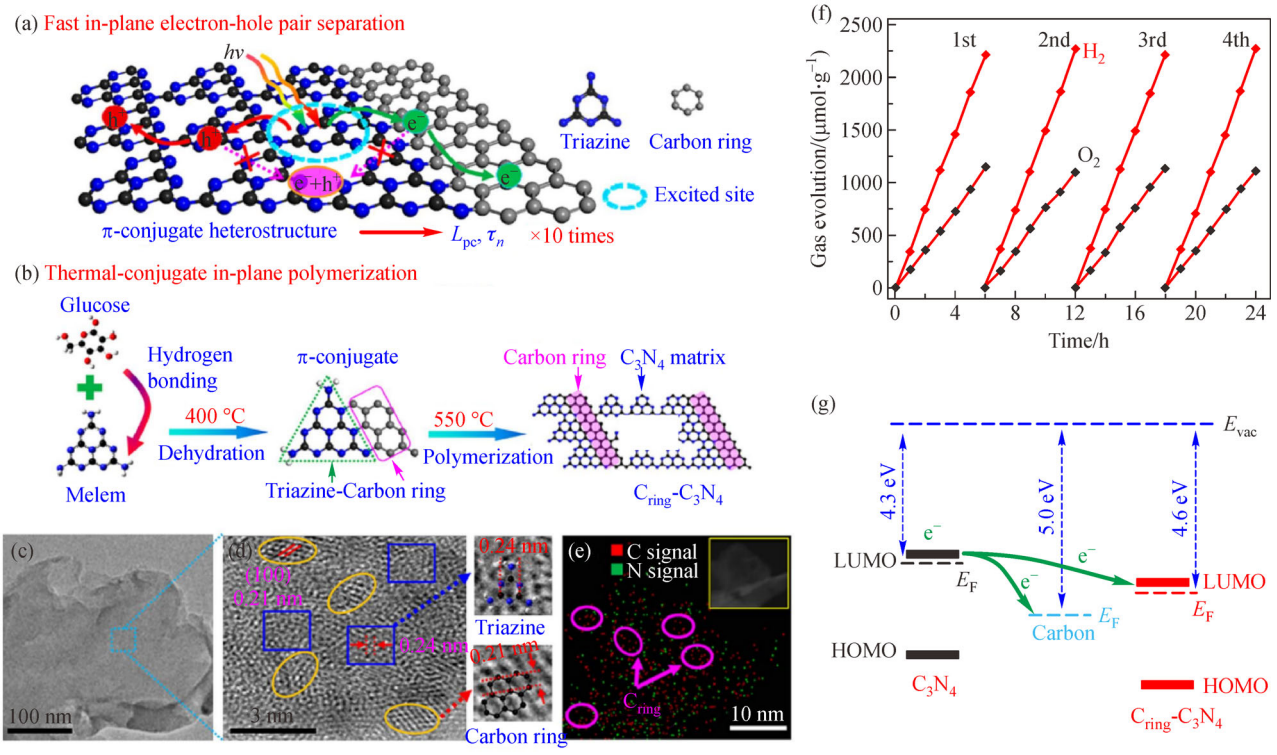

Fig. 6 Heterostructural carbon rings modified CN for photocatalytic overall water splitting.

(a) Schematic for photo-induced carrier transfer in (C_{ring})-CN, where L_{pc} and τ_n represent the photocarrier diffusion length and lifetime, respectively; (b) synthetic route for the in-plane heterostructure of (C_{ring})-CN; (c) TEM image; (d) HRTEM image for the sample (the elliptic area represents carbon ring, and the rectangular area is CN matrix.); (e) EDS mapping of (C_{ring})-CN (the inset of TEM image shows the corresponding region for mapping.); (f) time course of H_2 and O_2 evolution for (C_{ring})-CN ($\lambda > 420$ nm); (g) Fermi energy level profile for pristine CN, carbon, and (C_{ring})-CN (reproduced with permission from Ref. [63]).

electron-hole pair separation and photoelectrons transportation are therefore effectively expedited because of the local in-plane π-conjugated electric field. The photo-carrier diffusion length and lifetime are synergistically elongated by 10 times relative to the untreated CN. Eventually, the (C_{ring})-CN gives a prominent H_2 production rate of up to 11.13 μmol/h under full simulated solar light and a notable AQY of 5% at 420 nm. In addition, carbon-rich CN nanosheet (C_{co}-CN) is prepared by a combination processes, including the hydrothermal co-crystallization of terephthalic acid (TPA) with melamine (MA), and the following two-step thermal treatment and liquid exfoliation processes [64]. In the hydrothermal co-crystallization step, the orderly molecular self-assembly of the precursor tailors the chemical composition and electronic structure of the finally obtained C_{co}-CN. It exhibits an excellent photocatalytic overall water splitting ability by simultaneous producing H_2 and O_2 of up to 15.9 and 7.65 μmol/h in the absence of sacrificial reagents and cocatalysts. The improved separation efficiency, shortened transfer distance, and prolonged lifetime of photogenerated charge carrier are attributed to the promoted performance compared to that of pristine CN. Furthermore, the co-polymerization of MA, 2,4,6-triaminopyrimidine, and 1,3,5-triaminobenzene, containing few-carbon (pyrimidine) to all-carbon (benzene) aromatic rings, can substitute triazine rings by benzene aromatic rings [65]. The formation of N vacancies extends the π-electron conjugation in the 2D planar system and reduces the band gap to 2.1 eV with the negative shifts of energy band edges. Localized charge densities over valence band maximum (VBM) and conduction band minimum (CBM) in different regions of heptazine rings effectively decrease the charge carrier recombination rate. Ultimately, benzene ring incorporated CN directly splits pure water and generates about 7 μmol/h of H_2 with an AQY of 1.6% at 450 nm. Additionally, CN deprotonation by a small fraction of Na^+ renders the overall splitting water ability under visible light ($\lambda > 420$ nm) [66]. The substitution of protons by Na^+ completely prohibits the formation of H_2O_2, which is the dominant oxidation product in the case of pristine CN. The H_2 and O_2 production rates of Na-CN are 31.5 and 15.2 μmol/h (AQY: 1.45% at 420 nm; STH: 0.28%).

Moreover, elemental doping modulates the electronic structure of a material by introducing impurity energy levels into the band gap. It can effectively extend light absorption and tune chemical/physical properties, eventually endow desired properties for a specified photocatalyst. Consequently, elemental doping has been extensively investigated in photocatalysis [67–69]. However, it may not be a very useful method to make CN possess an overall water splitting ability because it has been rarely reported. Cui et al. synthesized B/K co-doped CN by using a recyclable molten-salt method and investigated its overall water splitting performance under visible light ($\lambda > 400$ nm) [70]. B/K co-doping significantly modulates the HOMO and the lowest unoccupied molecular orbitals (LUMO), and thus leads to an enhanced photo-induced carrier separation efficiency. Additionally, co-doping also promotes the resistance of H_2O_2 toxicity of CN. Compared to CN and K doped CN, B/K co-doped CN exhibits the highest water vapor splitting performance with a H_2 and O_2 production rate of 1.18 μmol/h and 0.58 μmol/h, respectively.

4.2.2 Crystallinity regulation

Insufficient crystallinity and accompanying negative effects are the well-known limitations of CN in photocatalysis. Bulk defects can act as recombination centers and heavily restrict photo-induced charge separation and migration. Improving crystallinity is a useful strategy to decrease defect density and tune electronic structure, thus reducing the carrier recombination and modulating the light harvesting ability [71]. Crystalline CN has been exploited in half photocatalytic H_2 production reaction [71–74]. The thermally calcining of the mixture of KCl, LiCl, and CN is frequently employed to improve crystallinity associating with enhanced electron-hole separation and migration efficiency. Wang et al. have comprehensively investigated the effect of pre-treated temperature on the crystallinity and catalytic activity of the final product [72]. Furthermore, exfoliating the good crystalline bulk into nanosheets can significantly improve the half H_2 evolution rate to 53 μmol/h under visible light ($\lambda > 420$ nm), which is 66 times that of pristine CN [74]. Other progresses on crystallinity CN can be referred to in Ref. [71]. Recently, crystallinity CN is developed for photocatalytic overall water splitting. For instance, Wang et al. successfully used surface kinetic control to photocatalyze pure water splitting by a covalent CN semiconductor with a crystalline poly(triazine imide) (PTI) framework (Fig. 7) [75]. The loading of a Pt is inevitable in water reduction and the co-deposition of a cobalt species can further increase the H_2 and O_2 production, as well enhancing the stability. Recently, the surface area ratios have been tuned and the reactive facets of crystalline CN have been identified [76]. The photogenerated electron-hole pairs can easily migrate along the conjugated layers to the $\{10\bar{1}0\}$ facets, and the co-catalysts are mostly photodeposited on the $\{10\bar{1}0\}$ facets due to the more-available electrons or holes on the prismatic surfaces. The above two factors confirm that the prismatic surfaces are the primary reactive facets. Moreover, PTI-550 gives a 189 μmol/h of H_2 production rate under full spectrum light irradiation (AQY: 8% at 365 nm).

4.3 Constructing nanocomposites

Combining CN with other semiconductors can remarkably improve charge separation/migration efficiency and extend light absorption. To the authors' knowledge, three types of

junctions (Type II, Z-scheme, and p-n junction, shown in Fig. 8) have been successfully constructed over CN to photocatalyze pure water splitting. The three heterojunctions demonstrate a staggered band structure between two components. The CN composited photocatalysts for overall water splitting have been reviewed in Table 3.

Table 3 CN based heterostructured photocatalysts for overall water splitting

Sample	Conditions	Efficiency	HER/(μmol·h^{-1})	H_2/O_2	Mass/mg	Other cocatalysts	Ref.
CoO/CN	LED, $\lambda > 400$ nm	NA	2.51	1.81	50	None	[77]
CoO Nanorod/CN	300 W Xe lamp, $\lambda > 400$ nm	AQY: 2.9% not mention the light wavelength	54	2.16	30	3 wt% Pt	[78]
2D/2D $Co_3(PO_4)_2$/CN	300 W Xe lamp, $\lambda > 400$ nm	AQY: 1.32% at 420 nm	18.78	2.12	50	None	[79]
LaOCl-Coupled CN	300 W Xe lamp	AQY: 0.4% at 380 nm	22.3	2.08	50	0.5 wt% Pt and 0.2 wt% CoO_x	[80]
P25/CN	Xe lamp	AQY: 0.96% at 350 nm	3.742	About 2.00	10	2 wt% Pt	[81]
MnO_x/CN/TiO_2/Au	300 W Xe lamp, $\lambda > 420$ nm	NA	4.8	2.04	100	None	[82]
CdS/Ni_2P/CN	300 W Xe lamp, $\lambda > 420$ nm	NA	0.778	2.01	50	None	[83]
MnO_x/CN/CdS/Pt	300 W Xe lamp	NA	65.17	2.03	50	None	[84]
MnO_x/CN/CdS/Pt	300 W Xe lamp, $\lambda > 400$ nm	AQY: 3.39% at 400 nm	9.244	2.01	10	None	[85]
CdSe QDs/P-CN	300 W Xe lamp, $\lambda > 420$ nm	NA	5.65	2.04	50	1 wt% Pt	[86]
CN (3 wt% Pt) – NaI – WO_3 (0.5 wt% Pt)	300 W Xe lamp	NA	22.2	2.00	300	None	[87]
CN (3 wt% Pt) – NaI – WO_3 (0.5 wt% Pt)	300 W Xe lamp, $\lambda > 395$ nm	NA	6.36	1.93	300	None	[87]
CN/$BiVO_4$, Fe^{2+} /Fe^{3+}	300 W Xe lamp	AQY: 1.8% at 420 nm	81.6	2.02	50	2 wt% Pt	[88]
2D α-Fe_2O_3/CN	300 W Xe lamp, $\lambda > 400$ nm	NA	1.91	2.00	50	3 wt% Pt 0.1 wt% RuO_2	[89]
Mn doped Fe_2O_3/CN	300 W Xe lamp, $\lambda > 400$ nm	NA	51	2.05	30	1 wt% Pt	[90]
Fe_2O_3/rGO/CN	300 W Xe lamp, $\lambda > 400$ nm	NA	43.6	2.06	40	Pt	[92]
CN@a-Fe_2O_3/Co-Pi	300 W Xe lamp, $\lambda > 420$ nm	NA	0.196	NA	20	None	[93]
a-Fe_2O_3@MnO_2/CN	300 W Xe lamp, $\lambda > 190$ nm	NA	124	2.07	30	None	[94]
CN/$BiFeO_3$	125 W Hg lamp with an UV filter	NA	0.933	2.01	40	None	[95]
Mn defective MnO_2/ Monolayer CN	300 W Xe lamp, $\lambda > 400$ nm	NA	1.212	2.10	20	3 wt% Pt	[96]
$WO_3 \cdot H_2O$/CN	300 W Xe lamp, $\lambda > 420$ nm	AQY: 6.2% at 420 nm	48.2	2.07	100	None	[97]
WO_3/rGO/CN	250 W halide lamp, $\lambda > 420$ nm	AQY: 0.9% at 420 nm	2.84	1.95	200	1 wt% Pt	[98]
$BiVO_4$/CN	300 W Xe lamp, $\lambda > 400$ nm	NA	15.6	2.14	100	3 wt% Pt	[99]
TiO_2/CN/WO_3/β-$Ni(OH)_2$/	150W Xe lamp; NaI as redox mediator	AQY: 2.04% at 425 nm	50.2	2.07	100	1 wt% Pt PtO_x	[101]
CN p-n homojunction/Ti_3C_2	300 W Xe lamp, $\lambda > 420$ nm	AQY: 8.7% at 350 nm	6.271	2.05	10	3 wt% Pt	[108]

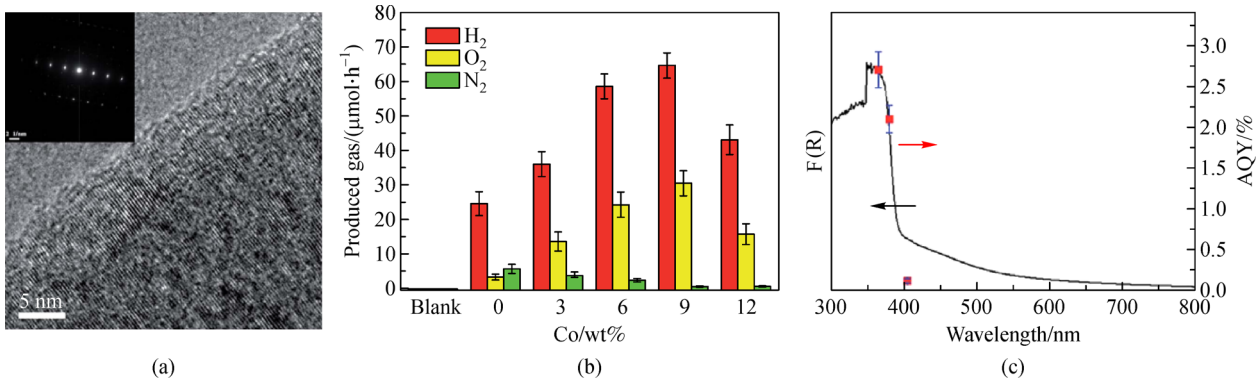

Fig. 7 Photocatalytic overall water splitting by a crystalline poly(triazine imide) (PTI) framework.
(a) HRTEM image of PTI·HCl (inset: the SAED pattern of the (002) plane); (b) photocatalytic overall water splitting of PTI·HCl under full spectrum light irradiation (1 wt% Pt as co-catalyst except for the blank one); (c) wavelength-dependent AQY of PTI·HCl loaded with 1 wt% Pt and 9 wt% Co (reproduced with permission from Ref. [75]).

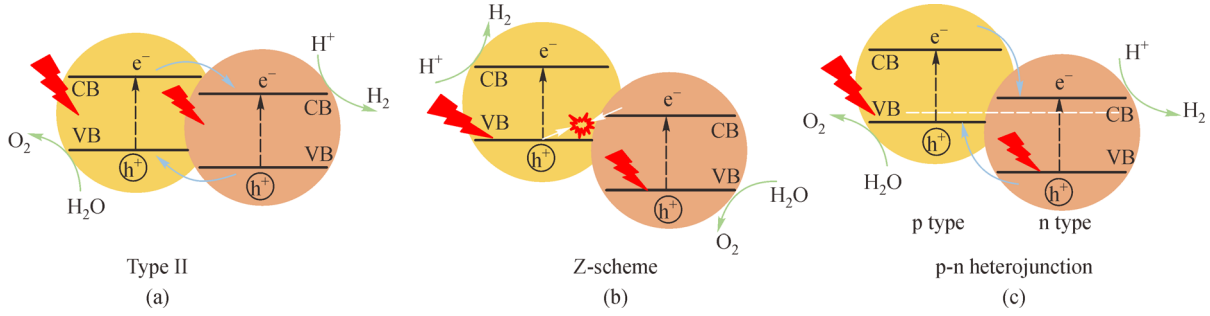

Fig. 8 Three types of junctions for photocatatlytic overall water splitting.
(a) Type II; (b) Z-scheme; (c) p-n heterojunction.

4.3.1 Type II

In Type II heterojunction (Fig. 8(a)), photo-induced electrons in the more negative CB of the OER component are injected into the CB of the HER component, while the holes in the VB of the HER component would be transferred to the VB of the OER component. As a result, electrons and holes are spatially remained in respective reservoirs, therefore improving their separation efficiency and further the water splitting performance. However, the reduction ability of photo-induced electrons and the oxidation ability of holes would be weakened to some extent after separation, representing a smaller driving force for each reaction.

Metal oxide semiconductors are potential candidates to construct heterojunctions with CN for photocatalytic overall water splitting. For example, in the CoO/CN heterojunction, synthesized by the one-step solvothermal method, the 2D CN nanosheet offers a large specific surface area to load CoO particles to prevent their aggregation [77]. The intimate contact of two components results in the formation of Type II energy band alignment and notably enhances charge utilization efficiency. Importantly, the introduction of CoO keeps CN from being poisoned by the H_2O_2 formed. Therefore, complementary advantages of two components enable durable stability after combination. Identically, the CoO nanorod/CN composite also demonstrates overall water splitting in the presence of Pt under visible light [78]. Moreover, integrating two layered materials to fabricate large-area 2D/2D heterojunction with desired functions may realize the photocatalytic overall water splitting. To this end, the 2D/2D $Co_3(PO_4)_2$/CN heterojunction, assembled by Coulomb electrostatic interaction, broadens the light absorption and concurrently accelerates the interfacial charge transfer, thus promoting the conversion of solar energy to H_2 [79]. The optimal sample has a 18.78 and 8.86 μmol/h of H_2 and O_2 production rate, respectively, and exhibits a prominent stability and recyclability. Corresponding AQY is 1.32% at 420 nm. Recently, it is reported that in order to keep the equilibrium of Fermi level differences of LaOCl and CN (Fig. 9), charge redistribution would happen after tight contact of two components [80]. The built-in interfacial electric field related to charge redistribution accelerates charge separation and migration. Ultimately, with the co-assistance of Pt and CoO_x, 22.3 and 10.7 μmol/h of H_2 and O_2 production rates are achieved under full-spectrum simulated light irradiation, respectively.

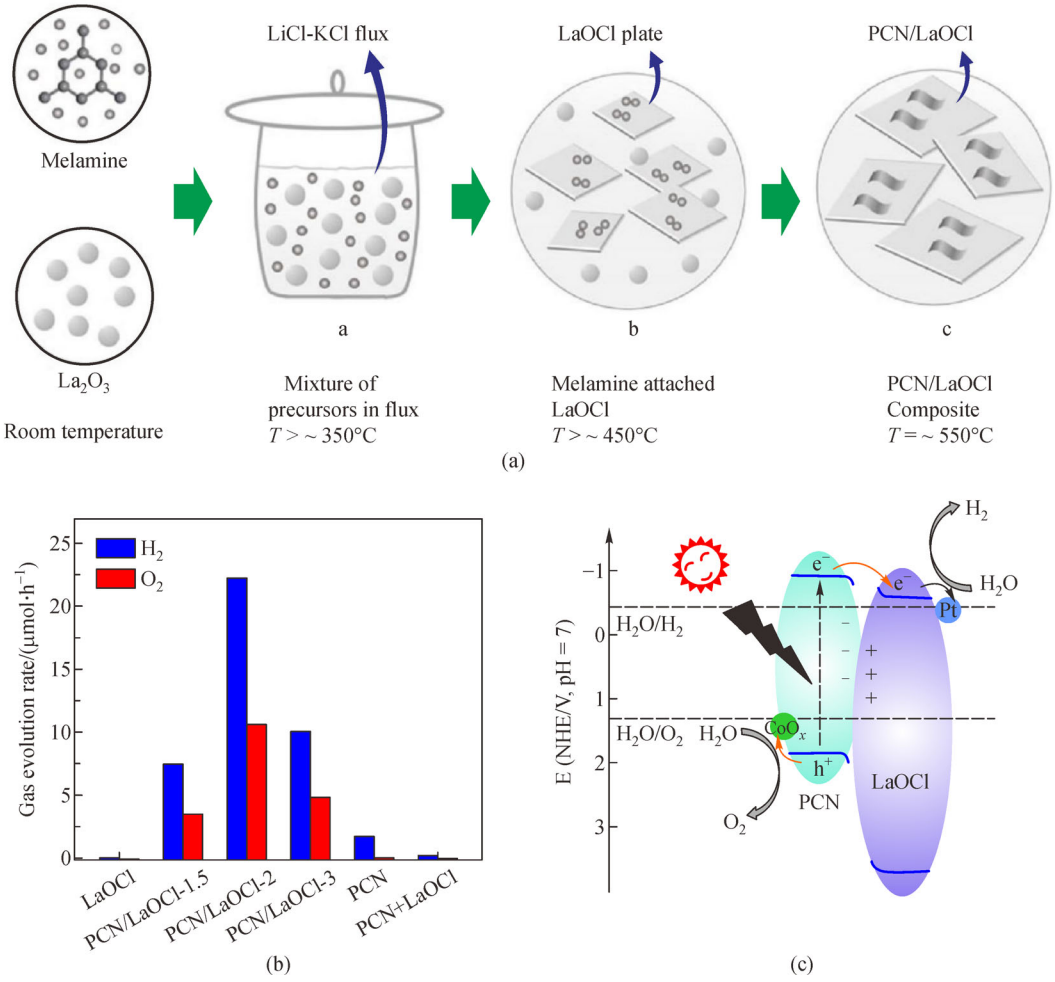

Fig. 9 Type II LaOCl/CN heterojunction for photocatalytic overall water splitting.
(a) Molten salt synthesis process of PCN/LaOCl composite; (b) photocatalytic overall water splitting activities over LaOCl, PCN/LaOCl-x (x = 1.5, 2, and 3), PCN, and PCN + LaOCl samples; (c) proposed mechanism of photocatalytic overall water splitting over PCN/LaOCl (reproduced with permission from Ref. [80]).

Regarding the composites containing CN and anatase/rutile TiO_2 (P25), the P25/CN multi-heterostructure displays a full-spectrum photocatalytic overall water splitting activity with a H_2 evolution rate of 3.742 μmol/h (AQY: 0.96% at 350 nm and 0.71% at 400 nm), which is 8 and 4 times that of CN and P25, respectively [81]. The rutile TiO_2 CB accepts electrons from the anatase TiO_2 and CN, while holes accumulate on the CN VB. The strengthened charge separation promises more carriers to participate in surface chemical redox reactions. Furthermore, with the co-decoration of MnO_x and Au, the Type II heterojunction of CN/TiO_2 also splits pure water splitting under solar light [82].

Besides oxides, chalcogenides are another kind of potential materials to construct Type II photocatalysts with CN. For example, the binary Type II heterojunction of CdS/CN shows a pure water splitting capacity under visible light. Further, intercalating Ni_2P between CdS and CN to function as a charge bridge can significantly accelerate the charge transfer from the CB of CN to that of CdS [83]. Therefore, a 0.778 and 0.388 μmol/h of H_2 and O_2 production rate over $CdS/Ni_2P/CN$ ternary junction is respectively obtained with a good stability. The activity is 4.02 times that of binary CdS/CN. In the hollow core/shell MnO_x/CN/CdS/Pt heterostructure, prepared by a continuous chemical-annealing-photoreduction method, the hollow microstructure provides abundant sites for photocatalytic redox reactions. Besides, the Type II energy band alignment between CN and CdS prominently promotes the photo-generated charge carrier separation/transport efficiency. Moreover, Pt particles deposited on CdS quickly accept the light-induced electrons, simultaneously, MnO_x excites hole-related species and accelerates H_2O_2 decomposition. Therefore, this delicately designed composite exhibits a remarkable overall water splitting performance with a 65.17 and 32.08 μmol/h of H_2 and O_2 evolution rate [84]. Similarly, the Pt and MnO_x dual cocatalysts deposited CN/CdS system fabricated via *in situ* photo-deposition

method also decomposes pure water under visible light ($\lambda > 400$ nm), with H_2 production rate up to 9.244 μmol/h and O_2 production rate of 4.60 μmol/h [85]. Additionally, the coupling P doped CN with CdSe quantum dots (QDs) could significantly extend light absorption of up to 700 nm, thus producing more charge carriers under the same light irradiation compared to the pristine CN [86]. P doping shifts CN CBM to a lower position than that of CdSe QDs, enabling photo-induced electrons to flow from CdSe to P doped CN and therefore improving the charge carrier separation/migration efficiency. Extended solar spectrum utilization and more efficient charge separation make CdSe QDs/P doped CN photocatalyst possess an overall water splitting ability under visible light ($\lambda > 420$ nm), where the H_2 and O_2 evolution rate are 5.65 and 2.78 μmol/h, respectively. In spite of the good overall water splitting performance of chalcogenides/CN photocatalysts, the chemical instability and serious photo-corrosion of chalcogenides are the two main constrains in large scale utilization. Moreover, the leakage of highly toxic heavy-metals (Cd, Pb, etc.) into environment would be detrimental to the environment and human health.

4.3.2 Z-scheme

Compared to the Type II system, the Z-scheme system enables a high charge-separation efficiency and simultaneously keeps a strong redox ability. As shown in Fig. 8(b), the photo-produced electrons in the OER catalyst CB are transferred to recombine with the holes in the HER catalyst VB via a redox mediator or at the interface. With respect to the CN based Z-scheme system, CN is always employed as the HER component due to its suitable potential for water reduction. In another word, a Z-scheme system can be constructed over CN by introducing an OER catalyst. Potential OER photocatalysts are Fe_2O_3, WO_3, $BiVO_4$, TiO_2, MnO_2, etc. At the beginning, Fe^{2+}/Fe^{3+} and I^-/IO_3^-, etc. are generally employed as liquid redox mediators. Then, all-solid-state Z-scheme with a better physical contact is developed to keep the highly efficient charge transfer of two components for better catalytic performance.

Inspired by the natural photosynthesis system, Tang et al. designed a photosynthesis-like composited overall water splitting system by combining CN with metal oxides ($BiVO_4$ and WO_3), with the assistance of redox mediators ($FeCl_2$, $FeCl_3$, and NaI) [87], in which, the best catalytic performance can be achieved when WO_3 is used as the OER component. In detail, under the full spectrum irradiation of a 300 W Xe lamp, CN (3 wt% Pt) – NaI – WO_3 (0.5 wt% Pt) displays a H_2 and O_2 production rate of 22.2 and 11.1 μmol/h, respectively. Under light with $\lambda > 395$ nm, the H_2 and O_2 production rate are 6.36 and 3.30 μmol/h, respectively. In addition to the effect of OER component, redox mediators also have notable influences on activity. Both in the cases of NaI and $FeCl_2$ solution, water splitting reaction happens directly at the start of light irradiation. When $FeCl_3$ is used as the redox mediator, no H_2 could be detected until a 15 h irradiation due to the production of Fe^{2+}/Fe^{3+} couple. In another case, the 3D mesoporous CN prepared by SiO_2 hard template, $BiVO_4$, and Fe^{2+}/Fe^{3+} are respectively used as HER component, OER component, and redox mediator in a Z-scheme system [88]. Porous structure enlarges the specific surface area, hence providing more reaction sites and shortening the charge transfer distance. The porous structure is also beneficial for the Fe^{2+}/Fe^{3+} pairs adsorption to collect the two components of a Z-scheme. Under full spectrum light irradiation, a 81.6 and 40.4 μmol/h of H_2 and O_2 evolution rate is respectively obtained.

Unlike the nature inspired photosynthesis II process, all-solid-state Z-scheme heterostructures are constructed without liquid redox mediators. Up to the present, all-solid-state CN based Z-scheme photocatalysts have been extensively investigated in the overall water splitting field. For example, the composite integrated by 2D α-Fe_2O_3 and 2D CN works as Z-scheme overall water splitting catalyst [89]. The 2D structure keeps short transfer distance of photo-induced charge carriers during the migration process from photocatalyst to reactant. At the same time, the intimate contact of two layered components enables fast and efficient electron transfer from α-Fe_2O_3 CB to CN VB, thus supressing the recombination possibility. In spite of the Z-scheme band alignment between Fe_2O_3 and CN, doping Mn into Fe_2O_3 crystal structure can evidently improve the conductivity, which is beneficial for charge transportation [90]. Accordingly, after combining Mn doped Fe_2O_3 nanocube with CN, the charge carrier density and the corresponding transfer efficiency are significantly improved, leading to the good overall water splitting performance. On the other hand, inserting an excellent charge mediator into HER and OER components is desired to thoroughly modulate charge transportation properties of a solid-state Z-scheme photocatalytic system [91]. As a proof of concept, Wang et al. selected reduced graphene oxide (rGO) as a solid conductor and successfully fabricated an all-solid-state Z-scheme system of CN/rGO/Fe_2O_3 [92]. Particularly, rGO is a 2D carbon material with a high specific surface area, an excellent electron transport mobility, and a chemically stable surface. The rGO nanosheets link the Fe_2O_3 nanoparticles and the CN nanosheets by chemical bonds and π-π stacking. The improved photocurrent density and evident PL quenching confirm that the rGO nanosheets remarkably accelerate interfacial charge transfer. Compared to CN, the CN/rGO/Fe_2O_3 has a 2-fold improvement of water splitting performance with a 43.6 μmol/h of H_2 evolution. Generally, the water oxidation process is the rate-determining step of the overall reaction. Reasonably, adding cocatalyt to accelerate the OER process should be effective for improving the overall performance. In the CN/α-Fe_2O_3 Z-scheme system, depositing Co-Pi on α-Fe_2O_3 to

collect and store holes successfully realizes the overall water splitting under visible light ($\lambda > 420$ nm) [93]. However, the H_2 production rate of 0.196 μmol/h is fairly slow. Then, the hierarchical Fe_2O_3@MnO_2 core/shell nanocube was used to combine with CN to form a Z-scheme photocatalyst, which exhibits a 124 and 60 μmol/h of H_2 and O_2 production rate, respectively [94]. In this ternary heterojunction, Fe_2O_3 and MnO_2, first forming a Type II structure, leads to the rapid transfer of photo-excited holes from MnO_2 VB to Fe_2O_3 VB. Then, the Z-scheme band structure between Fe_2O_3@MnO_2 and CN makes the electron in MnO_2 CB to combine with the hole from CN. Eventually, this ternary composite gives a preferable photocatalytic H_2 production of 124 μmol/h. In addition to Fe_2O_3, $BiFeO_3$ as OER catalyst has been successfully integrated with CN to form a Z-scheme heterojunction [95]. The binary composite achieves H_2 and O_2 production from pure water under full spectrum light illumination due to the facilitated electron-hole separation and migration.

The redox cycling properties of multivalent metal cation can work as an electron mediator in the solid-state Z-scheme photocatalytic system. For instance, in the case of Mn^{3+} defective MnO_2 modified CN heterojunction, in addition to the OER catalyst role of MnO_2 (Fig. 10), Mn^{3+} cations containing in MnO_2 on the one hand promote H_2O adsorption and on the other hand simultaneously intrigue redox cycle reaction with Mn^{4+} [96]. The redox cycle reaction of Mn^{3+}/Mn^{4+} enables a notably strengthened charge separation/migration efficiency. Finally, the H_2 and O_2 generation rate is realized as 1.212 and 0.578 μmol/h, respectively. The $WO_3 \cdot H_2O$ nanosheets can absorb sufficient visible light due to the approximate 2.4 eV band gap, and also is responsible for OER because of the suitable valence band edge potential of nearly 3.45 V [97]. Accordingly, the Van der Waals heterojunction of $WO_3 \cdot H_2O$/CN has been facilely prepared by using the hydrothermal method to split pure water. In this Z-scheme system, the electrons in the CB of $WO_3 \cdot H_2O$ and the holes in the VB of CN recombine at the interface of the two components. On the other hand, the photo-induced holes of $WO_3 \cdot H_2O$ would accumulate on its VB, and the photo-induced electrons of CN would be retained on its CB. The evidently reduced charge carrier recombination therefore renders a considerable photocatalytic overall water splitting performance, in which the average H_2 and O_2 generation rates reach roughly 48.2 and 23.2 μmol/h, respectively. Compared to the CN/WO_3 binary system, introducing rGO between the two components can further enhance the activity [98]. Furthermore, the 2D Z-scheme $BiVO_4$/CN photocatalytst has been prepared by using a two-step hydrothermal/calcination method [99]. In this work, the electron spin resonance (ESR) analysis, by comparing the signal intensities of hydroxyl radical ($\cdot OH$) and superoxide radical ($\cdot O_2^-$) in the case of CN, $BiVO_4$, and $BiVO_4$/CN, was used to verify the Z-scheme mechanism. Finally, as aforementioned, TiO_2 and CN can form Type II heterojunction to improve the photocatalytic performance [81,100]. Further, Liu and co-workers used Type II TiO_2/CN heterostructure as the HER component to couple with an OER catalyst (WO_3 and $BiVO_4$) to successfully construct a Z-scheme multi-heterostructures for overall water splitting [101]. Compared to TiO_2 or CN, TiO_2/CN gives a more efficient H_2 production activity in the half reaction. Eventually, the hybrid system, integrated TiO_2/CN with β-$Ni(OH)_2$/WO_3, achieves an overall water splitting performance with a 50.2 and 24.3 μmol/h of H_2 and O_2 evolution rate (AQY: 2.06% at 425 nm), respectively, in the presence of HER cocatalyst (Pt) and redox mediator (5 mmol/L NaI).

4.3.3 p-n junction

Type II heterojunction can ideally separate electron-hole pairs, but the enhancement is always not sufficient to

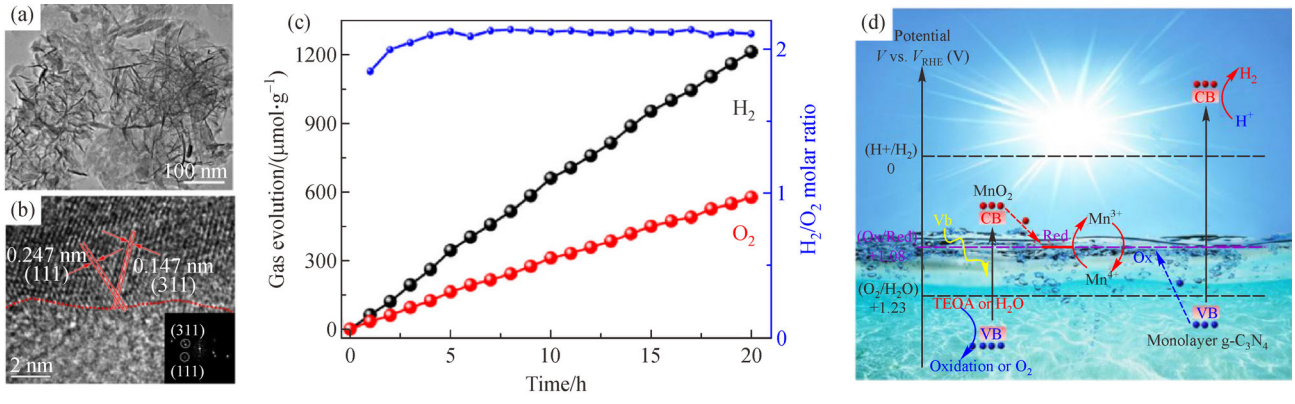

Fig. 10 Z-scheme MnO_2/CN heterojunction for photocatalytic overall water splitting.
(a) Preparation process of MnO_2/Monolayer CN; (b) TEM image; (c) HRTEM image of MnO_2/Monolayer CN; (d) overall water spitting performance of MnO_2/Monolayer CN under visible light irradiation, using Pt (3%) as a co-catalytst (reproduced with permission from Ref. [96]).

overcome the ultrafast electron-hole recombination. Consequently, in addition to the Z-scheme heterojunction, the p-n heterojunction concept has also been proposed to accelerate the electron-hole migration across the heterojunction by forming an interfacial electric field. Because of the Fermi level difference of p and n semiconductor, before light irradiation, the electrons on the n-type semiconductor tend to diffuse into the p-type semiconductor, meanwhile, the holes on the p-type semiconductor tend to diffuse into the n-type semiconductor, therefore respectively leaving a positively and negatively charged spaces at each side. As a result, the region close to p-n interface is charged. Under light irradiation and internal electric field, photo-generated electrons and holes will migrate directionally to the CB of n-type semiconductor and the VB of p-type semiconductor, respectively. Therefore, the electron-hole separation efficiency in p-n heterojunction is faster than that of Type II heterojunction due to the synergy effect of the strong internal electric field and band alignment [102,103].

In the research conducted in the past, p-n junctions for photocatalytic application are mainly developed over inorganic materials. Although CN is a typical n-type organic polymeric semiconductor, using it to construct p-n junction has attracted little concentration. Ye et al. found that the introduction of cyano terminal groups (C≡N) *in situ* transform CN from n-type to p-type, and thus forming the p-n homojunction [104]. The p-n homojunction of CN demonstrates better charge separation and transportation properties, and gives a 5 fold promoted photocatalytic H_2 production performance. In addition, CN based p-n heterojunctions for half photocatalytic H_2 production can refer to these work [105–107]. However, CN based p-n junctions are rarely reported for overall water splitting.

Recently, one piece of work relating to CN based p-n junction has been reported for photocatalytic overall water splitting [108], in which, the doping of P in CN crystal structure changes the n-type characteristic to p-type, and obviously decreases the surface energy by replacing original atoms. Furthermore, energy level redistribution makes the local charge carriers to be dominant by the holes. After integrating CN p-n homojunction with Ti_3C_2, the internal electric field at the p-n region and the secondary driving force between CN and Ti_3C_2 significantly prohibit the recombination and prolong the life time of charge carriers. Therefore, photocatalytic overall water splitting is achieved with a H_2 and O_2 production of 6.271 and 3.054 μmol/h, respectively.

5 Summary and outlook

In summary, up-to-date progress of CN based photocatalysts for overall water splitting by modification methods as following three aspects have been reviewed, including loading cocatalysts to bring in water reduction and oxidation sites and improve charge carrier utilization, regulating and modifying microstructure to positively modulate intrinsic properties relating to water splitting reaction, and constructing multicomponent nanocomposites to use more sun light and improve separation/transportation of the electron-hole pairs. Of course, each strategy may affect the photocatalytic reaction process from different aspects. In the future, more attention should be paid from the following perspectives to further improve the STH conversion efficiency.

Improving light harvesting ability. The theoretical maximum of the STH efficiency of a photocatalyst highly relates to the band gap value. For the one-step photoexcitation system, the STH efficiency should reach 10% at least in terms of producing H_2 with an acceptable cost. However, it is impossible to meet this target for a photocatalyst with an absorption edge of around 500 nm, even with an AQY of 100% [8]. Unfortunately, the gap value of CN is about 2.7 eV, corresponding the absorption edge of around 460 nm, which does not fulfill the basic requirement of light absorption. Consequently, it is of great value to extend the light absorption and further study the photocatalytic water splitting on the light absorption strengthened CN. In addition to self-modification, integrating with broader light absorption ability materials, such as plasmonics and small band gap semiconductors, etc. may be available to improve the solar light absorption capacity of CN based photocatalysts.

Developing efficient cocatalysts. Although many cocatalysts have been developed to facilitate overall water splitting, there still exists much space for further improvement. In the studies at present, noble metals are almost contained both in HER and OER cocatalysts. Therefore, designing noble metal free cocatalysts with an excellent cocatalytic performance and stability is crucial for large-scale application. On the other hand, the H_2O_2 formed during pure water splitting sometimes poison the catalysts, thus decreasing catalytic activity versus reaction time. That is to say, designing and fabricating a cocatalyst with the ability to rapidly decompose H_2O_2 and concurrently prohibit the back reaction of water splitting should be of great significance. In recent years, numerous researches have been conducted on pure water splitting for H_2 and H_2O_2 production [109–110], where H_2 separates automatically with H_2O_2. Therefore, this novel system realizes pure water splitting under solar light and concurrently avoids the separation of H_2 and O_2 relative to conventional system. Furthermore, compared to O_2 production, H_2O_2 formation is more thermodynamically preferable because of the two-electron process. As a consequence, designing H_2O_2 formation cocatalysts may be applicable for STH improvement.

Theoretical prediction and *in situ* experimental investigation. Using DFT calculation to screen potential materials that endow more efficient charge separation/transportation and improved light absorption after combing with CN should be valuable. Of course, the theoretical

method is also suitable for designing novel cocatalysts and predict property changes after modulating of a photocatalyst. Moreover, photocatalytic overall water splitting is still in a state of chaos, restricting the efficient photocatalyst design. Constructing *in situ* experimental apparatus to monitor the transient progress of water splitting should be useful but challenging, and theoretical calculation is a strong method to further explore the keys of mechanism beyond experiments.

Acknowledgements This work was supported by the National Key Research and Development Program of China (No. 2018YFB1502000); the National Natural Science Foundation of China (Grant Nos. 51961130386, 51876173, 62074123, and 61701543); Newton Advanced Fellowship of the Royal Society (No. NAF\R1\191163); the PetroChina Innovation Foundation (No. 2019D-5007-0410); and the China Postdoctoral Science Foundation (2020M683472).

References

1. Hisatomi T, Kubota J, Domen K. Recent advances in semiconductors for photocatalytic and photoelectrochemical water splitting. Chemical Society Reviews, 2014, 43(22): 7520–7535
2. Moniz S J A, Shevlin S A, Martin D J, et al. Visible-light driven heterojunction photocatalysts for water splitting – a critical review. Energy & Environmental Science, 2015, 8(3): 731–759
3. Fujishima A, Honda K. Electrochemical photolysis of water at a semiconductor electrode. Nature, 1972, 238(5358): 37–38
4. Luo J, Im J H, Mayer M T, et al. Water photolysis at 12.3% efficiency via perovskite photovoltaics and earth-abundant catalysts. Science, 2014, 345(6204): 1593–1596
5. Jia J, Seitz L C, Benck J D, et al. Solar water splitting by photovoltaic-electrolysis with a solar-to-hydrogen efficiency over 30%. Nature Communications, 2016, 7(1): 13237
6. Chen Y, Feng X, Liu Y, et al. Metal oxide-based tandem cells for self-biased photoelectrochemical water splitting. ACS Energy Letters, 2020, 5(3): 844–866
7. Chen X, Shen S, Guo L, et al. Semiconductor-based photocatalytic hydrogen generation. Chemical Reviews, 2010, 110(11): 6503–6570
8. Chen S, Takata T, Domen K. Particulate photocatalysts for overall water splitting. Nature Reviews. Materials, 2017, 2(10): 17050
9. Wang Z, Li C, Domen K. Recent developments in heterogeneous photocatalysts for solar-driven overall water splitting. Chemical Society Reviews, 2019, 48(7): 2109–2125
10. Wang Q, Hisatomi T, Jia Q, et al. Scalable water splitting on particulate photocatalyst sheets with a solar-to-hydrogen energy conversion efficiency exceeding 1%. Nature Materials, 2016, 15 (6): 611–615
11. Maeda K, Takata T, Hara M, et al. GaN: ZnO solid solution as a photocatalyst for visible-light-driven overall water splitting. Journal of the American Chemical Society, 2005, 127(23): 8286–8287
12. Maeda K, Domen K. Solid solution of GaN and ZnO as a stable photocatalyst for overall water splitting under visible light. Chemistry of Materials, 2010, 22(3): 612–623
13. Melo M A Jr, Wu Z, Nail B A, et al. Surface photovoltage measurements on a particle tandem photocatalyst for overall water splitting. Nano Letters, 2018, 18(2): 805–810
14. Wang Q, Nakabayashi M, Hisatomi T, et al. Oxysulfide photocatalyst for visible-light-driven overall water splitting. Nature Materials, 2019, 18(8): 827–832
15. Zheng D, Cao X N, Wang X. Precise formation of a hollow carbon nitride structure with a Janus surface to promote water splitting by photoredox catalysis. Angewandte Chemie International Edition, 2016, 55(38): 11512–11516
16. Ong W J, Tan L L, Ng Y H, et al. Graphitic carbon nitride (g-C_3N_4)-based photocatalysts for artificial photosynthesis and environmental remediation: are we a step closer to achieving sustainability? Chemical Reviews, 2016, 116(12): 7159–7329
17. Thomas A, Fischer A, Goettmann F, et al. Graphitic carbon nitride materials: variation of structure and morphology and their use as metal-free catalysts. Journal of Materials Chemistry, 2008, 18(41): 4893–4908
18. Niu P, Zhang L, Liu G, et al. Graphene-like carbon nitride nanosheets for improved photocatalytic activities. Advanced Functional Materials, 2012, 22(22): 4763–4770
19. Kang Y, Yang Y, Yin L C, et al. Selective breaking of hydrogen bonds of layered carbon nitride for visible light photocatalysis. Advanced Materials, 2016, 28(30): 6471–6477
20. Zheng Y, Lin L, Wang B, et al. Graphitic carbon nitride polymers toward sustainable photoredox catalysis. Angewandte Chemie International Edition, 2015, 54(44): 12868–12884
21. Luo B, Song R, Jing D. Significantly enhanced photocatalytic hydrogen generation over graphitic carbon nitride with carefully modified intralayer structures. Chemical Engineering Journal, 2018, 332: 499–507
22. Luo B, Song R, Geng J, et al. Strengthened spatial charge separation over Z-scheme heterojunction photocatalyst for efficient photocatalytic H_2 evolution. Applied Surface Science, 2019, 475: 453–461
23. Luo B, Song R, Geng J, et al. Facile preparation with high yield of a 3D porous graphitic carbon nitride for dramatically enhanced photocatalytic H_2 evolution under visible light. Applied Catalysis B: Environmental, 2018, 238: 294–301
24. Wang X, Maeda K, Thomas A, et al. A metal-free polymeric photocatalyst for hydrogen production from water under visible light. Nature Materials, 2009, 8(1): 76–80
25. Yu H, Shi R, Zhao Y, et al. Alkali-assisted synthesis of nitrogen deficient graphitic carbon nitride with tunable band structures for efficient visible-light-driven hydrogen evolution. Advanced Materials, 2017, 29(16): 1605148
26. Wang X, Maeda K, Thomas A, et al. A metal-free polymeric photocatalyst for hydrogen production from water under visible light. Nature Materials, 2009, 8(1): 76–80
27. Kim I Y, Jo Y K, Lee J M, et al. The unique advantages of exfoliated 2D nanosheets for tailoring the functionalities of nanocomposites. Journal of Physical Chemistry Letters, 2014, 5 (23): 4149–4161
28. Yang S, Gong Y, Zhang J, et al. Exfoliated graphitic carbon nitride nanosheets as efficient catalysts for hydrogen evolution under visible light. Advanced Materials, 2013, 25(17): 2452–2456

29. Ma R, Liu Z, Li L, et al. Exfoliating layered double hydroxides in formamide: a method to obtain positively charged nanosheets. Journal of Materials Chemistry, 2006, 16(39): 3809–3813
30. Niu P, Zhang L, Liu G, et al. Graphene-like carbon nitride nanosheets for improved photocatalytic activities. Advanced Functional Materials, 2012, 22(22): 4763–4770
31. Li Y, Jin R, Xing Y, et al. Macroscopic foam-like holey ultrathin g-C_3N_4 nanosheets for drastic improvement of visible-light photocatalytic activity. Advanced Energy Materials, 2016, 6(24): 1601273
32. Yang J, Wang D, Han H, et al. Roles of cocatalysts in photocatalysis and photoelectrocatalysis. Accounts of Chemical Research, 2013, 46(8): 1900–1909
33. Bai J, Lu B, Han Q, et al. (111) facets-oriented Au-decorated carbon nitride nanoplatelets for visible-light-driven overall water splitting. ACS Applied Materials & Interfaces, 2018, 10(44): 38066–38072
34. Wang N, Li X. Protonated carbon nitride nanosheet supported IrO_2 quantum dots for pure water splitting without sacrificial reagents. Inorganic Chemistry Frontiers, 2018, 5(9): 2268–2275
35. Zhang G, Lan Z A, Lin L, et al. Overall water splitting by Pt/g-C_3N_4 photocatalysts without using sacrificial agents. Chemical Science (Cambridge), 2016, 7(5): 3062–3066
36. Pan Z, Zheng Y, Guo F, et al. Decorating CoP and Pt nanoparticles on graphitic carbon nitride nanosheets to promote overall water splitting by conjugated polymers. ChemSusChem, 2017, 10(1): 87–90
37. Pan Z, Wang S, Niu P, et al. Photocatalytic overall water splitting by spatially-separated Rh and RhO_x cocatalysts on polymeric carbon nitride nanosheets. Journal of Catalysis, 2019, 379: 129–137
38. Zeng Z, Quan X, Yu H, et al. Alkali-metal-oxides coated ultrasmall Pt sub-nanoparticles loading on intercalated carbon nitride: enhanced charge interlayer transportation and suppressed back-wark reaction for overall water splitting. Journal of Catalysis, 2019, 377: 72–80
39. Sun S, Feng Y, Pan L, et al. Integrating Pt@$Ni(OH)_2$ nanowire and Pt nanoparticle on C_3N_4 with fast surface kinetics and charge transfer towards highly efficient photocatalytic water splitting. Applied Catalysis B: Environmental, 2019, 259: 118028
40. Yan J, Wu H, Chen H, et al. One-pot hydrothermal fabrication of layered β-$Ni(OH)_2$/g-C_3N_4 nanohybrids for enhanced photocatalytic water splitting. Applied Catalysis B: Environmental, 2016, 194: 74–83
41. Sun S, Zhang Y C, Shen G, et al. Photoinduced composite of Pt decorated $Ni(OH)_2$ as strongly synergetic cocatalyst to boost H_2O activation for photocatalytic overall water splitting. Applied Catalysis B: Environmental, 2019, 243: 253–261
42. Li X, Bi W, Zhang L, et al. Single-atom Pt as co-catalyst for enhanced photocatalytic H_2 evolution. Advanced Materials, 2016, 28(12): 2427–2431
43. Lee B H, Park S, Kim M, et al. Reversible and cooperative photoactivation of single-atom Cu/TiO_2 photocatalysts. Nature Materials, 2019, 18(6): 620–626
44. Fang X, Shang Q, Wang Y, et al. Single Pt atoms confined into a metal–organic framework for efficient photocatalysis. Advanced Materials, 2018, 30(7): 1705112
45. Liu M, Wang L, Zhao K, et al. Atomically dispersed metal catalysts for the oxygen reduction reaction: synthesis, characterization, reaction mechanisms and electrochemical energy applications. Energy & Environmental Science, 2019, 12(10): 2890–2923
46. Zhang Q, Guan J. Recent progress in single-atom catalysts for photocatalytic water splitting. Solar RRL, 2020, 4(9): 2000283
47. Qureshi M, Garcia-Esparza A T, Jeantelot G, et al. Catalytic consequences of ultrafine Pt clusters supported on $SrTiO_3$ for photocatalytic overall water splitting. Journal of Catalysis, 2019, 376: 180–190
48. Su H, Liu M, Cheng W, et al. Heterogeneous single-site synergetic catalysis for spontaneous photocatalytic overall water splitting. Journal of Materials Chemistry A, Materials for Energy and Sustainability, 2019, 7(18): 11170–11176
49. Wang S, Chen L, Zhao X, et al. Efficient photocatalytic overall water splitting on metal-free 1D SWCNT/2D ultrathin C_3N_4 heterojunctions via novel non-resonant plasmonic effect. Applied Catalysis B: Environmental, 2020, 278: 119312
50. Liu J, Liu Y, Liu N, et al. Metal-free efficient photocatalyst for stable visible water splitting via a two-electron pathway. Science, 2015, 347(6225): 970–974
51. Qu D, Liu J, Miao X, et al. Peering into water splitting mechanism of g-C_3N_4-carbon dots metal-free photocatalyst. Applied Catalysis B: Environmental, 2018, 227: 418–424
52. Fu Y, Liu C, Zhu C, et al. High-performance NiO/g-C_3N_4 composites for visible-light-driven photocatalytic overall water splitting. Inorganic Chemistry Frontiers, 2018, 5(7): 1646–1652
53. Han M, Wang H, Zhao S, et al. One-step synthesis of CoO/g-C_3N_4 composites by thermal decomposition for overall water splitting without sacrificial reagents. Inorganic Chemistry Frontiers, 2017, 4 (10): 1691–1696
54. Liu J, Liu N Y, Li H, et al. A critical study of the generality of the two step two electron pathway for water splitting by application of a C_3N_4/MnO_2 photocatalyst. Nanoscale, 2016, 8(23): 11956–11961
55. Wang N, Li J, Wu L, et al. MnO_2 and carbon nanotube co-modified C_3N_4 composite catalyst for enhanced water splitting activity under visible light irradiation. International Journal of Hydrogen Energy, 2016, 41(48): 22743–22750
56. Zhou X, Li J, Cai X, et al. *In situ* photo-derived MnOOH collaborating with Mn_2Co_2C@C dual co-catalysts boost photocatalytic overall water splitting. Journal of Materials Chemistry A, Materials for Energy and Sustainability, 2020, 8(33): 17120–17127
57. Liu W, Cao L, Cheng W, et al. Single-site active cobalt-based photocatalyst with a long carrier lifetime for spontaneous overall water splitting. Angewandte Chemie International Edition, 2017, 56(32): 9312–9317
58. Xiong Y, Chen Y, Yang N, et al. WC_{1-x}-coupled 3D porous defective g-C_3N_4 for efficient photocatalytic overall water splitting. Solar RRL, 2019, 3(5): 1800341
59. Chen X, Shi R, Chen Q, et al. Three-dimensional porous g-C_3N_4 for highly efficient photocatalytic overall water splitting. Nano Energy, 2019, 59: 644–650
60. Zeng Y, Li H, Luo J, et al. Sea-urchin-structure g-C_3N_4 with

narrow bandgap (~2.0 eV) for efficient overall water splitting under visible light irradiation. Applied Catalysis B: Environmental, 2019, 249: 275–281
61. Song T, Zhang P, Wang T, et al. Alkali-assisted fabrication of holey carbon nitride nanosheet with tunable conjugated system for efficient visible-light-driven water splitting. Applied Catalysis B: Environmental, 2018, 224: 877–885
62. Wu C, Xue S, Qin Z, et al. Making g-C_3N_4 ultra-thin nanosheets active for photocatalytic overall water splitting. Applied Catalysis B: Environmental, 2021, 282: 119557
63. Che W, Cheng W, Yao T, et al. Fast photoelectron transfer in (C_{ring})-C_3N_4 plane heterostructural nanosheets for overall water splitting. Journal of the American Chemical Society, 2017, 139(8): 3021–3026
64. Fang X, Gao R, Yang Y, et al. A cocrystal precursor strategy for carbon-rich graphitic carbon nitride toward high-efficiency photocatalytic overall water splitting. Science, 2019, 16: 22–30
65. Bellamkonda S, Shanmugam R, Gangavarapu R R. Extending the π-electron conjugation in 2D planar graphitic carbon nitride: efficient charge separation for overall water splitting. Journal of Materials Chemistry A, Materials for Energy and Sustainability, 2019, 7(8): 3757–3771
66. Guo F, Chen J, Zhang M, et al. Deprotonation of g-C_3N_4 with Na ions for efficient nonsacrificial water splitting under visible light. Journal of Materials Chemistry A, Materials for Energy and Sustainability, 2016, 4(28): 10806–10809
67. Zhang G, Zhang M, Ye X, et al. Iodine modified carbon nitride semiconductors as visible light photocatalysts for hydrogen evolution. Advanced Materials, 2014, 26(5): 805–809
68. Liu C, Zhang Y, Dong F, et al. Chlorine intercalation in graphitic carbon nitride for efficient photocatalysis. Applied Catalysis B: Environmental, 2017, 203: 465–474
69. Li J, Cui W, Sun Y, et al. Directional electron delivery via a vertical channel between g-C_3N_4 layers promotes photocatalytic efficiency. Journal of Materials Chemistry A, Materials for Energy and Sustainability, 2017, 5(19): 9358–9364
70. Wang J C, Hou Y, Feng F D, et al. A recyclable molten-salt synthesis of B and K co-doped g-C_3N_4 for photocatalysis of overall water vapor splitting. Applied Surface Science, 2021, 537: 148014
71. Lin L, Yu Z, Wang X. Crystalline carbon nitride semiconductors for photocatalytic water splitting. Angewandte Chemie International Edition, 2019, 58(19): 6164–6175
72. Lin L, Ren W, Wang C, et al. Crystalline carbon nitride semiconductors prepared at different temperatures for photocatalytic hydrogen production. Applied Catalysis B: Environmental, 2018, 231: 234–241
73. Schwinghammer K, Mesch M B, Duppel V, et al. Crystalline carbon nitride nanosheets for improved visible-light hydrogen evolution. Journal of the American Chemical Society, 2014, 136 (5): 1730–1733
74. Ou H, Lin L, Zheng Y, et al. Tri-s-triazine-based crystalline carbon nitride nanosheets for an improved hydrogen evolution. Advanced Materials, 2017, 29(22): 1700008
75. Lin L, Wang C, Ren W, et al. Photocatalytic overall water splitting by conjugated semiconductors with crystalline poly(triazine imide) frameworks. Chemical Science (Cambridge), 2017, 8(8): 5506–5511
76. Lin L, Lin Z, Zhang J, et al. Molecular-level insights on the reactive facet of carbon nitride single crystals photocatalysing overall water splitting. Nature Catalysis, 2020, 3(8): 649–655
77. Guo F, Shi W, Zhu C, et al. CoO and g-C_3N_4 complement each other for highly efficient overall water splitting under visible light. Applied Catalysis B: Environmental, 2018, 226: 412–420
78. Wang N, Li X. Facile synthesis of CoO nanorod/C_3N_4 heterostructure photocatalyst for an enhanced pure water splitting activity. Inorganic Chemistry Communications, 2018, 92: 14–17
79. Shi W, Li M, Huang X, et al. Facile synthpolymeric carbon nitride for overall water splitting through a one-photon excitation pathway. Angewandte Chemie International Edition, 2020, 59: 1–6
80. Lin Y, Su W, Wang X, et al. LaOCl-coupled polymeric carbon nitride for overall water splitting through a one-photon excitation pathway. Angewandte Chemie International Edition, 2020, 59: 1–6
81. Fang Y, Huang W, Yang S, et al. Facile synthesis of anatase/rutile TiO_2/g-C_3N_4 multi-heterostructure for efficient photocatalytic overall water splitting. International Journal of Hydrogen Energy, 2020, 45(35): 17378–17387
82. Raziq F, Sun L, Wang Y, et al. Synthesis of large surface-area g-C_3N_4 comodified with MnO_x and Au-TiO_2 as efficient visible-light photocatalysts for fuel production. Advanced Energy Materials, 2018, 8(3): 1701580
83. He H, Cao J, Guo M, et al. Distinctive ternary CdS/Ni_2P/g-C_3N_4 composite for overall water splitting: Ni_2P accelerating separation of photocarriers. Applied Catalysis B: Environmental, 2019, 249: 246–256
84. Pan J, Wang P, Wang P, et al. The photocatalytic overall water splitting hydrogen production of g-C_3N_4/CdS hollow core–shell heterojunction via the HER/OER matching of Pt/MnO_x. Chemical Engineering Journal, 2021, 405: 126622
85. Zhou X, Fang Y, Cai X, et al. *In situ* photodeposited construction of Pt–CdS/g-C_3N_4–MnO_x composite photocatalyst for efficient visible-light-driven overall water splitting. ACS Applied Materials & Interfaces, 2020, 12(18): 20579–20588
86. Raziq F, Hayat A, Humayun M, et al. Photocatalytic solar fuel production and environmental remediation through experimental and DFT based research on CdSe-QDs-coupled P-doped-g-C_3N_4 composites. Applied Catalysis B: Environmental, 2020, 270: 118867
87. Martin D J, Reardon P J T, Moniz S J A, et al. Visible light-driven pure water splitting by a nature-inspired organic semiconductor-based system. Journal of the American Chemical Society, 2014, 136(36): 12568–12571
88. Chen W, Liu M, Li X, et al. Synthesis of 3D mesoporous g-C_3N_4 for efficient overall water splitting under a Z-scheme photocatalytic system. Applied Surface Science, 2020, 512: 145782
89. She X, Wu J, Xu H, et al. High efficiency photocatalytic water splitting using 2D α-Fe_2O_3/g-C_3N_4 Z-scheme catalysts. Advanced Energy Materials, 2017, 7(17): 1700025
90. Wang N, Han B, Wen J, et al. Synthesis of novel Mn-doped Fe_2O_3 nanocube supported g-C_3N_4 photocatalyst for overall visible-light driven water splitting. Colloids and Surfaces A, Physicochemical and Engineering Aspects, 2019, 567: 313–318

91. Favereau L, Makhal A, Pellegrin Y, et al. A molecular tetrad that generates a high-energy charge-separated sate by mimicking the photosynthetic Z-scheme. Journal of the American Chemical Society, 2016, 138(11): 3752–3760
92. Pan Z, Zhang G, Wang X. Polymeric carbon nitride/reduced graphene oxide/Fe_2O_3: all-solid-state Z-scheme system for photocatalytic overall water splitting. Angewandte Chemie International Edition, 2019, 58(21): 7102–7106
93. Sun Y, Shao S, Wang Y, et al. Fabrication of hollow g-C_3N_4@α-Fe_2O_3/Co-Pi heterojunction spheres with enhanced visible-light photocatalytic water splitting activity. International Journal of Hydrogen Energy, 2020, 45(4): 2840–2851
94. Wang N, Wu L, Li J, et al. Construction of hierarchical Fe_2O_3@MnO_2 core/shell nanocube supported C_3N_4 for dual Z-scheme photocatalytic water splitting. Solar Energy Materials and Solar Cells, 2020, 215: 110624
95. Sepahvand H, Sharifnia S. Photocatalytic overall water splitting by Z-scheme g-C_3N_4/$BiFeO_3$ heterojunction. International Journal of Hydrogen Energy, 2019, 44(42): 23658–23668
96. Mo Z, Xu H, Chen Z, et al. Construction of MnO_2/Monolayer g-C_3N_4 with Mn vacancies for Z-scheme overall water splitting. Applied Catalysis B: Environmental, 2019, 241: 452–460
97. Yang Y, Qiu M, Li L, et al. A direct Z-scheme van der waals heterojunction ($WO_3 \cdot H_2O$/g-C_3N_4) for high efficient overall water splitting under visible-light. Solar RRL, 2018, 2(9): 1800148
98. Zhao G, Huang X, Fina F, et al. Facile structure design based on C_3N_4 for mediator-free Z-scheme water splitting under visible light. Catalysis Science & Technology, 2015, 5(6): 3416–3422
99. Xie H, Zhao Y, Li H, et al. 2D $BiVO_4$/g-C_3N_4 Z-scheme photocatalyst for enhanced overall water splitting. Journal of Materials Science, 2019, 54(15): 10836–10845
100. Tan S, Xing Z, Zhang J, et al. Ti^{3+}-TiO_2/g-C_3N_4 mesostructured nanosheets heterojunctions as efficient visible-light-driven photocatalysts. Journal of Catalysis, 2018, 357: 90–99
101. Yan J, Wu H, Chen H, et al. Fabrication of TiO_2/C_3N_4 heterostructure for enhanced photocatalytic Z-scheme overall water splitting. Applied Catalysis B: Environmental, 2016, 191: 130–137
102. Pan L, Wang S, Xie J, et al. Constructing TiO_2 p-n homojunction for photoelectrochemical and photocatalytic hydrogen generation. Nano Energy, 2016, 28: 296–303
103. Low J, Yu J, Jaroniec M, et al. Heterojunction photocatalysts. Advanced Materials, 2017, 29(20): 1601694
104. Liu G, Zhao G, Zhou W, et al. *In situ* bond modulation of graphitic carbon nitride to construct p–n homojunctions for enhanced photocatalytic hydrogen production. Advanced Functional Materials, 2016, 26(37): 6822–6829
105. Shi J W, Zou Y, Cheng L, et al. *In-situ* phosphating to synthesize Ni_2P decorated NiO/g-C_3N_4 p-n junction for enhanced photocatalytic hydrogen production. Chemical Engineering Journal, 2019, 378: 122161
106. Nekouei F, Nekouei S, Pouzesh M, et al. Porous-CdS/Cu_2O/graphitic-C_3N_4 dual p-n junctions as highly efficient photo/catalysts for degrading ciprofloxacin and generating hydrogen using solar energy. Chemical Engineering Journal, 2020, 385: 123710
107. Hua S, Qu D, An L, et al. Highly efficient p-type Cu_3P/n-type g-C_3N_4 photocatalyst through Z-scheme charge transfer route. Applied Catalysis B: Environmental, 2019, 240: 253–261
108. Ai Z, Shao Y, Chang B, et al. Rational modulation of p-n homojunction in P-doped g-C_3N_4 decorated with Ti_3C_2 for photocatalytic overall water splitting. Applied Catalysis B: Environmental, 2019, 259: 118077
109. Zhang K, Wang L, Sheng X, et al. Tunable bandgap energy and promotion of H_2O_2 oxidation for overall water splitting from carbon nitride nanowire bundles. Advanced Energy Materials, 2016, 6(11): 1502352
110. Xue F, Si Y, Wang M, et al. Toward efficient photocatalytic pure water splitting for simultaneous H_2 and H_2O_2 production. Nano Energy, 2019, 62: 823–831